Catena 259 (2025) 109355

Contents lists available at ScienceDirect

Catena

journal homepage: www.elsevier.com/locate/catena

Effect of rainfall event on water-dispersible colloids in a hyper-arid Atacama alluvial fan

Xiaolei Sun [a,b,c,*], Simon Matthias May [d], Alain Mollier [c], Miaoyue Zhang [e], Qian Zhang [f], Bárbara Fuentes [g], Franko Arenas [h], Roland Bol [a], Erwin Klumpp [a]

[a] Institute of Bio- and Geosciences, Agrosphere (IBG-3), Forschungszentrum Jülich 52425 Jülich, Germany
[b] Institute for Environmental Research, RWTH Aachen University, Worringerweg 1, 52074 Aachen, Germany
[c] ISPA, Bordeaux Sciences Agro, INRAE, 33140 Villenave d'Ornon, France
[d] Institute of Geography, University of Cologne, Albertus-Magnus-Platz, 50923 Cologne, Germany
[e] School of Environmental Science and Engineering, Guangdong Provincial Key Laboratory of Environ. Pollut. Control and Remediation Technology, Sun Yat-sen University, 510006 Guangzhou, PR China
[f] State Key Laboratory of Pollution Control and Resource Reuse, School of Environment, Nanjing University, 210023 Nanjing, China
[g] Departamento de Ingeniería Química y de Medio Ambiente, Universidad Católica del Norte, Antofagasta, Chile
[h] Programa de Doctorado en Ciencias mención Geología, Departamento de Ciencias Geológicas, Universidad Católica del Norte, Antofagasta, Chile

ARTICLE INFO

Keywords:
WDC-P
Soil aggregate breakdown
Leaching process
Subsurface flow
Hyper-arid region
Muti-age alluvial fan

ABSTRACT

Occasional extreme rainfall events significantly influence colloid dynamics and nutrient cycling in the hyper-arid Atacama Desert. We hypothesized that the response of water-dispersible soil colloids (WDCs, <300 nm) and their associated phosphorus (WDC-P) dynamics to water addition is controlled by soil aggregation/disintegration and transport processes influenced by soil age. We conducted an irrigation experiment (44.8 mm h^{-1} for 30 min) on an alluvial fan system at 1480 m a.s.L. in the Paposo that is characterized by two sections of different age. Soil aggregates and WDCs were analyzed before and after irrigation event using dry sieving and asymmetric flow field-flow fractionation (AF4). Although total WDCs and sub-fractions did not show statistically significant changes, full infiltration and lateral subsurface flow indicated that mobilization occurred. A negative correlation between WDCs and mean weight diameter (MWD) suggests that aggregate disintegration released colloids, which may have been offset by transport and implying a dynamic balance. This balance varied with sediment age and weathering. In the younger surface (0–1 cm), raindrop impact likely released fine colloids (FCs, 24–210 nm) by breaking weak aggregates, while ~32 % of deeper-layer WDCs (>1 cm) were mobilized or aggregated. In contrast, the older surface showed WDCs decline, likely due to higher clay content (7 %) and aggregate stability. Below 1 cm, swelling and clay dispersion contributed to WDCs accumulation. Soil age also affected WDC and nano-colloid (NCs, 0.6–24 nm) composition. Older soils were enriched in Al, Fe, and Si. Irrigation partially altered these patterns, increasing NC-Al in the younger fan. Notably, NC-P increased despite declining NCs, likely due to enhanced binding with Al (hydr)oxides, suggesting NC-P dynamics are governed by both content and composition of WDCs. These results highlight sediment age-dependent responses of WDCs and WDC-P to short-term water inputs and underscore their role in shaping nutrient fluxes and soil resilience in arid environments.

1. Introduction

Soil colloids primarily consist of a mixture or complexes of phyllosilicates, hydrous oxides of Si, Fe, and Al, and natural organic matter (Jiang et al., 2015; Missong et al., 2018a; Schumacher et al., 2005). They are recognized as the most chemically active size fraction in soils, with diameters ranging from 1 to 10^3 nm (Said-Pullicino et al., 2021; VandeVoort et al., 2013). Among them, water-dispersible colloids (WDCs, <500 nm) exhibit a strong tendency to disperse and transport within soils when water is present (Jiang et al., 2015; Missong et al., 2018a). WDCs have a high specific surface area and can act as sinks for nutrients such as phosphorus (P) and contaminants due to their strong adsorption characteristics (Ilg et al., 2008; Siemens et al., 2004; Yu et al., 2024). WDCs therefore play a fundamental role in soil fertility and

* Corresponding author at: ISPA, Bordeaux Sciences Agro, INRAE, 33140 Villenave d'Ornon, France.
E-mail address: xiaolei.sun@inrae.fr (X. Sun).

https://doi.org/10.1016/j.catena.2025.109355
Received 19 September 2024; Received in revised form 30 July 2025; Accepted 2 August 2025
Available online 9 August 2025

environmental governance (Menezes-Blackburn et al., 2021; Tian et al., 2023; Weber et al., 2009). The dynamics of WDCs and their associated P (WDC-P) have been extensively studied in moisture-rich ecosystems such as forest soils (Missong et al., 2018b; Tian et al., 2023; Wang et al., 2020b), arable lands (Jiang et al., 2015; Li et al., 2021a; Pan et al., 2023; Regelink et al., 2014), grasslands (Jiang et al., 2017), floodplains, and stream waters (Baken et al., 2016a, b; Gottselig et al., 2014, 2017; Weber et al., 2009). By contrast, the behavior of WDCs and WDC-P in hyper-arid environments—such as deserts—remains largely overlooked, despite the fact that even occassional and short-term water inputs (e.g., rainfall or irrigation) can rapidly mobilize soil colloids, causing erosion and nutrient cycling (Dunai et al., 2020). This is particularly critical in sensitive landscapes like the Chinese Loess Plateau, where fine particles, including WDCs, play an important role in soil degradation and downstream agricultural productivity (Liu et al., 2019; Wang et al., 2014). Therefore, understanding how WDCs and WDC-P respond to occasional rainfall event in arid regions is essential for predicting landform evolution, managing soil resources, and maintaining effective nutrient cycling under conditions of extreme water scarcity. Notably, in arid soils like those of the Atacama Desert, P is predominantly associated with colloids smaller than 300 nm (Moradi et al., 2020; Sun et al., 2023), which are also characterized by higher reactivity and mobility under episodic water inputs. To better capture the dynamics of this key fraction, we defined WDCs in this study as <300 nm, instead of the conventional <500 nm.

In arid and semi-arid regions, where vegetation is sparse or absent, water movement is governed primarily by evaporation, infiltration, and run-off (Meadows et al., 2008; Vereecken et al., 2022). Infiltration and run-off facilitate the lateral and downward transport of particles following rainfall or irrigation. In contrast, strong evaporation in desert systems drives upward water fluxes, carrying dissolved and colloidal particles toward the surface and leading to the accumulation of salt ions and WDCs in upper soil layers (Moradi et al., 2020; Sun et al., 2023; Voigt et al., 2020). This upward movement induces the formation of hardened layers or crusts, thereby altering soil structure and reducing permeability over time (Arens et al., 2021; Arenas-Díaz et al., 2022). In fact, these hydrological processes not only control the spatial redistribution of WDCs but also contribute to their mobilization by facilitating the breakdown of soil aggregates (Kjaergaard et al., 2004; Krause et al., 2020; Mohanty et al., 2015, 2016). Three primary mechanisms responsible for the breakdown of soil aggregates and thus WDC release include splash erosion caused by raindrops, slaking and swelling, and physicochemical weathering (Fernández-Raga et al., 2017; Kjaergaard et al., 2004; Liu et al., 2021). Raindrop splash on the soil surface is the first step for soil erosion by water, which is influenced by rainfall intensity and quantity as well as soil properties such as moisture, organic matter content, infiltration capacity, texture, and structure (Ayoubi et al., 2022; Hu et al., 2018; Li et al., 2021b). Slaking occurs when soil aggregates are unable to withstand the stress caused by rapid water uptake. The stress primarily originates from two sources: clay minerals swelling as water is absorbed, and internal pressure due to compressed air bubbles as water is drawn into small soil pores (Fajardo et al., 2016; Jones et al., 2021; Reichert et al., 2009). Indeed, clay content and soil structure can affect the slaking process, thus leading to the formation of particles on the macro and micro scales that facilitate water penetration (Artieda and Herrero, 2003). In contrast, aggregate destruction and the generation of fine particles during heavy rainfall contribute to the clogging of soil pores and the formation of crust, especially under dry conditions (Li et al., 2018). These phenomena subsequently reduce the infiltration capacity of the soil, leading to an increase in surface run-off (Vereecken et al., 2022), which can result in the loss of WDCs and WDC-P. Overall, in hyper-arid regions, the interplay between water-driven aggregate breakdown and soil hydraulic behavior has important but understudied implications for fine particle dynamics and nutrient cycling. During these processes, sediment age—through its control on clay content, surface sealing, and soil texture—emerges as a key factor shaping the sensitivity of soils to these processes (Hartmann et al., 2022; Walk et al., 2023).

In arid regions, water scarcity severely limits the chemical weathering of primary minerals and restricts the occurrence and spread of microbial life. Consequently, the soil P cycling is inhibited, resulting in P-limited ecosystems (Shen et al., 2020; Sun et al., 2024). However, P is often enriched in the WDCs, potentially through OC-Ca-P associations or by binding with Fe/Al (hydr)oxides or clay minerals (Wang et al., 2020b; Sun et al., 2023). Therefore, even in soils with sparse vegetation and limited biological activity, WDC-P can accumulate to relatively high concentrations, while total soil P remains comparable to that of surrounding areas (Moradi et al., 2020; Sun et al., 2023). This makes WDC-P a potentially more sensitive indicator of nutrient availability and even early life-supporting conditions. During prolonged dry periods, WDC-P generally follows a similar vertical distribution as WDCs accumulating in deeper soil layers in the absence of vegetation, and near the surface where sparse plant growth occurs (Moradi et al., 2020; Sun et al., 2023). However, occasional water availability triggers biotic processes that significantly impact on its cycling (Ewing et al., 2007; Knief et al., 2020; Wang et al., 2021a). These events may influence the mobilization and transformation of WDCs through chemical weathering, aggregation/dispersion, potentially altering their composition and, in turn, P associations (Gu et al., 2018; Wang et al., 2024). Therefore, whether WDC-P exhibits a similar trend with WDCs is unclear, highlighting the need for further investigation into its dynamics under water disturbance.

To explore how short-term water availability affects the behavior of WDCs and WDC-P in hyper-arid environments, we conducted an irrigation experiment in a multi-phase alluvial fan system in the Atacama Desert, which is one of the oldest and driest deserts on Earth. Understanding how soil functions, particularly in terms of biogeochemical P cycling, adapts to extreme water scarcity and excess events in the Atacama Desert provides valuable insights to address the ecological challenges posed by global desertification and climate change, as well as for defining the limits of life on Earth (Tian et al., 2023; Moradi et al., 2020; Sun et al., 2023). The study focused on two soil sections formed during distinct phases of alluvial fan development: a younger fan section (~14 ka), where active hydrological pathways allow for fluvial processes and colloid mobilization, and an older fan section (~56 ka), where long-term surface stabilization and crust formation inhibit water infiltration and particle transport. By analyzing WDCs and WDC-P dynamics in the upper soil layers (0–15 cm) before and after irrigation, we aimed to determine (1) whether WDC dynamics differ between the two sections, (2) how these differences relate to pedogenic properties such as clay content and soil structure, and (3) whether WDC-P responds in parallel with changes in WDC dynamics. We hypothesized that WDCs would be more mobile in the younger fan due to higher permeability and weaker aggregation, while the older fan would show limited response due to structural resistance linked to advanced weathering. Furthermore, we hypothesized that WDC-P may exhibit a response distinct from that of WDCs under water disturbance, possibly due to changes in WDC composition, which affect the nature and strength of P associations.

2. Methods and materials

2.1. The study site

The Atacama Desert in Chile, known for its extreme aridity and intense ultraviolet radiation, serves as an ideal analogue for tracing life in harsh terrestrial environments on Earth and Mars (Davis et al., 2009; Eshel et al., 2021; Georgiou et al., 2015). The Atacama Desert soil primarily forms through the accumulation of atmospheric dust deposition. The dynamics of fine particles, especially colloids therefore play a crucial role in shaping the topographic features and influencing element accumulation and nutrient cycling (Arenas-Díaz et al., 2022; Ewing et al., 2006; Li et al., 2019). Occasional rainfall events occurring during the El Niño–Southern Oscillation (ENSO) every few decades are one of

the major water sources for the region, resulting not only in the initiation of life but also facilitating unique landscape evolution processes (Cabré et al., 2020; Houston, 2006b; Jordan et al., 2020). In the Paposo region (approximately 25°0′52″S, 70°20′8″W, 1480 m a. s. L.) (Fig. 1), such rainfall events have shaped an alluvial fan system, which is selected as the study site. The climate at the site is classified as hyper-arid (aridity index: 1.2) with a mean annual temperature of 17.2 °C and mean annual precipitation of 3 mm (Quade et al., 2007; Sun et al., 2023; Zomer et al., 2022). The alluvial fan, characterized by a triangular shaped form, is approximately 80 m wide and around 200 m long (Fig. 1; Moradi et al., 2020; Sun et al., 2023). The entire system and its direct vicinity can be divided into four primary geomorphological units: bedrock, hillslope deposits/scree deposits, an older (inactive) alluvial fan generation, and a younger (active) alluvial fan generation (Sun et al., 2023; Fig. 1c). Optically stimulated luminescence (OSL) dating of sediments from the older and the younger fan generation was performed in a previous study (Sun et al., 2023) and resulted in ages of 13.6 ka (younger fan section) and 56.4 ka (older fan section; cf. Table S1; Sun et al., 2023). Notably, the older and younger fan sections are distinct and separated by a topographic step of ~0.8 m.

2.2. Irrigation experiment and sampling

The irrigation experiment and sample collection were conducted on 14th March 2019 on the alluvial fan system. Irrigation was performed on both the older and the younger fan sections, with three replications for each fan section (I1-6; Fig. 1). At each irrigation point, a 75 × 75 cm plot was set up (Fig. 2A, B). Irrigation was performed using a simple device consisting of a full-cone nozzle (Lechler, no. 490.608.30.CA.00.0) mounted 2 m above ground on an aluminum frame (Fig. 2C),

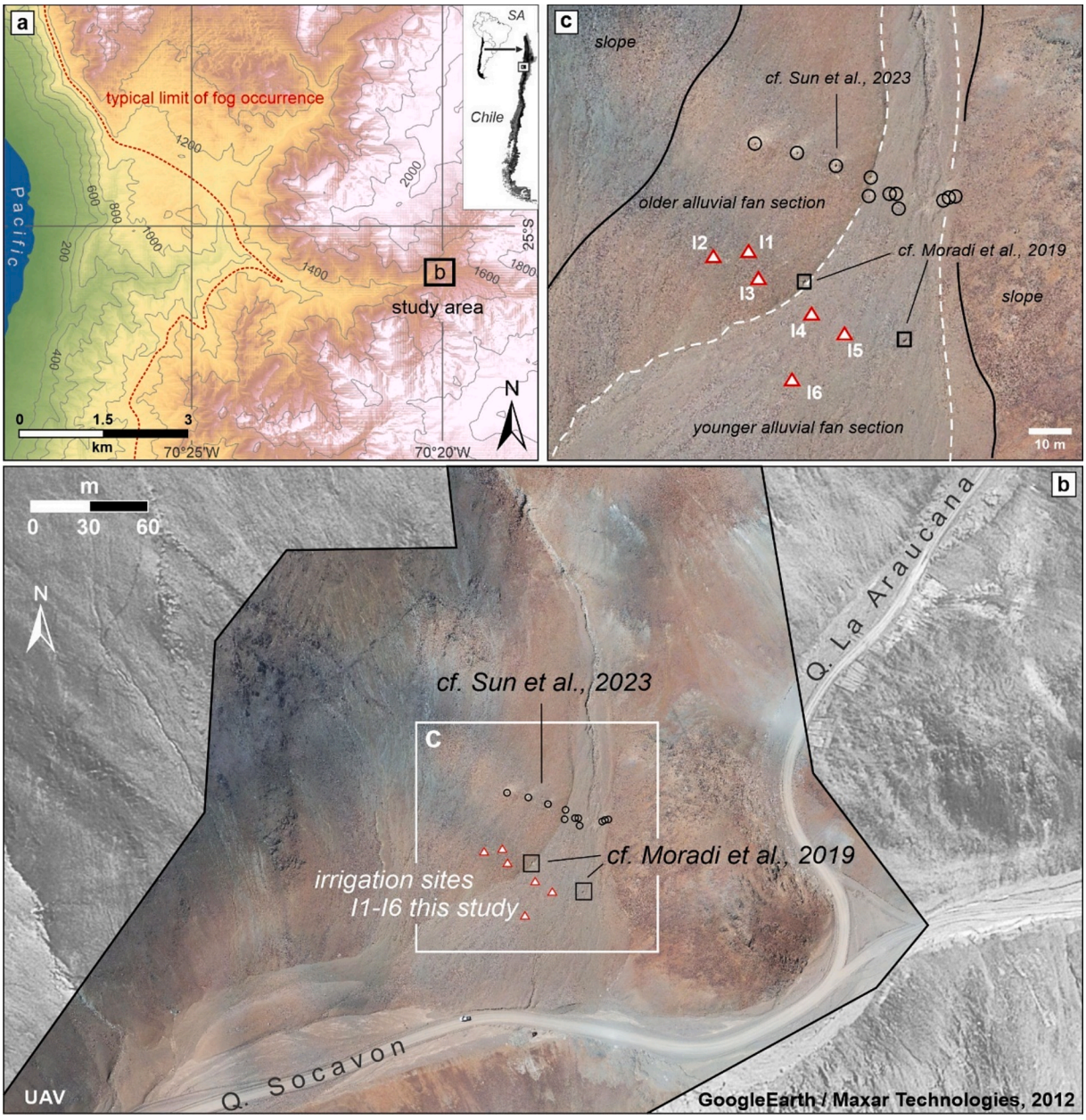

Fig. 1. Study area. (a) Digital elevation model (SRTM data, NASA) of the study area at 1480 m.a.s.L.; the upper limit of the fog bank is typically around 1100 m. (b & c) Position of soil profiles on the fan, showing the two different alluvial fan sections, with red colors dominating the abandoned (old) surface, and gray to brown colors indicating the younger and active fan section. Irrigation sites and samples I1, I2 and I3 are located in the older fan section and I4, I5, I6 in the younger fan section.

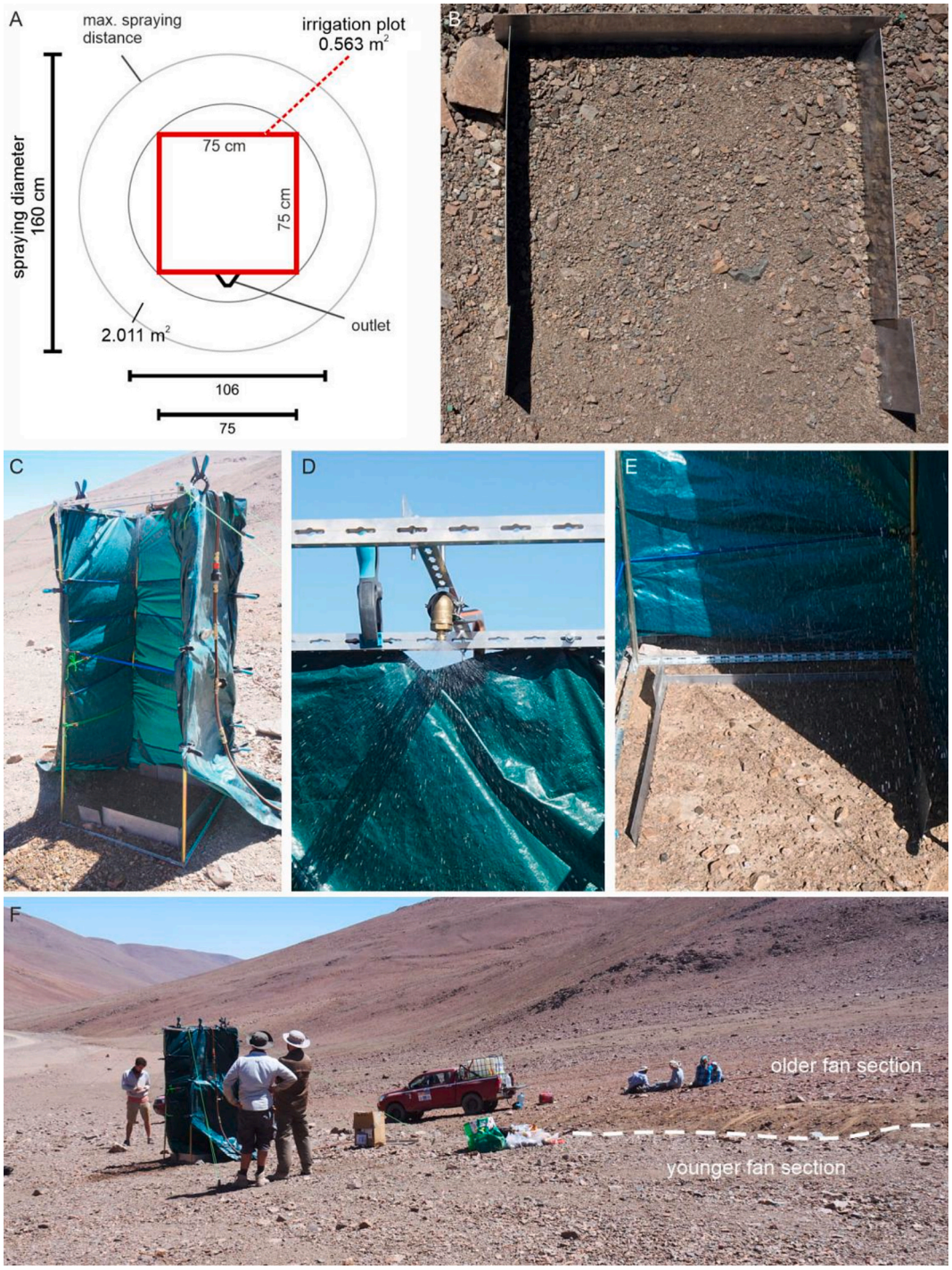

Fig. 2. Irrigation experiments. (A) The irrigation plot with an area of 75 × 75 cm^2. (B) Pre-irrigation photos of the irrigated surface. (C) Set-up of the irrigation device. (D) Full cone nozzle (Lechler, no. 490.609.30.CA.00.0) with a typical drop size range of <0.5 mm to 4.49 mm. A configuration with 1 nozzle operated with 0.8 bar was chosen. The flow rate was 44.8 mm h^{-1} during the 30 min-long experiment. (E) The irrigated plot during irrigation. (F) Overview of the setting with the irrigation device located on the younger alluvial fan surface; note the topographic step (white dashed line) between the younger and older fan sections.

surrounded by a canvas wind shield–although wind disturbance was generally negligible. The design of the irrigation system was adapted from other studies (Iserloh et al., 2012; May et al., 2020). It simulated natural rainfall using drops ranging from 0.5 to 4.49 mm in diameter, with fall velocities between 3 and 5 m s^{-1} – within the lower range of natural rainfall velocities (3–9 m s^{-1}; Iserloh et al. 2012; Cerdà, 1997) due to the 2 m drop height (Fig. 2D).

The system was therefore operated with a pressure of 0.8 bar to simulate an intense rainfall event (>10 L h^{-1} m^{-2}, Xie et al., 2021). The kinetic energy per drop (E) was estimated to range from 0.4 × 10^{-6} J to 7.4 × 10^{-4} J (Li et al., 2018). The nozzle was connected to a 1000 L water container filled with demineralized water by a hose system that was equipped with a manometer, a flow control unit, and a flow meter. According to a previous study (May et al., 2020), the water distribution of the spraying nozzle on the plot is homogeneous, which is expressed by a uniformity coefficient (UC) of 90.6 % (Christiansen, 1942; Iserloh et al. 2012). Each of the six plots was irrigated for 30 min, delivering 45 L of water over a spray area of 2.011 m^2 (diameter 160 cm), corresponding

to 12.6 and 44.8 L h^{-1} m^{-2} for the 0.563 m^2 plot area. Historical records indicated that the maximum rainfall rates in the region occurred at Antofagasta on June 18, 1991 (24 mm h^{-1}) and at Taltal on March 24–26, 2015 (48 mm h^{-1}) (Bozkurt et al., 2016; Pfeiffer et al., 2021). The artificial irrigation rate of 44.8 mm h^{-1} used in this study is therefore comparable to past rainfall events in the Paposo region.

Irrigation samples were collected from the top–left corner of each plot after the surface had visibly dried and no water residue remained (Fig. 3c). Correspondingly, control samples (non-irrigated) were collected approximately 25 cm upslope from wach irrigation point (Fig. 3c), resulting in a total of twelve sampling sites. At each site, soil samples were collected from the surface to a depth of 15 cm below the surface (b.s.), divided into four layers: 0–1 cm, 1–5 cm, 5–10 cm, and 10–15 cm (Fig. 3e, f). The 15 cm maximum depth was selected based on observed water percolation, which reached the 10–15 cm layer. In the older fan section, a clay-horizon was found at 5–10 cm. In the younger fan section, the leaching water penetrated deeper than in the older fan section, which was limited to a depth of 15 cm (Fig. 3d–f). Loose rocks and plant debris were removed prior to sampling, and spades and pickaxes were used to excavate the pits. The I3 site (older fan section), was dug down to 5 cm b.s. due to the presence of large rocks or hardpans beyond this depth.

2.3. Separation of soil aggregates by dry sieving

Dry sieving was used in the study to determine soil aggregates at the soil surface (0–1 cm) and in sub-surface soils (>1 cm) (Bach and Hofmockel, 2014), after air-drying for all samples both before and after irrigation. A stack of sieves, with mesh openings of 2 mm, 0.25 mm, 0.053 mm, and 0.02 mm, was shaken horizontally by hand at a rate of 30 times per minute for 2 min. Dry aggregates were gently removed from the sieves and then weighed to determine the distribution of soil aggregates.

The aggregate size distribution was characterized by mean weighted diameter of aggregates (MWD, mm) (Fomin et al., 2021):

$$\mathrm{MWD} = \frac{\sum(\mathrm{mi} \times \mathrm{Di})}{\sum \mathrm{mi}}$$

where i is number of aggregate fractions, m_i is the weight of i aggregate fraction (g), D_i is the diameter of i aggregate fraction calculated as the mean value of the mesh diameters of the upper and lower sieves (mm).

2.4. Extraction of water-dispersible colloids (WDCs)

The desert soils were dry in their natural environment before sampling. The irrigation soil samples were stored at room temperature. Due to the low clay content, no soil clods formed following irrigation, eliminating the need for mechanical disaggregation. They were subsequently sieved to a size smaller than 2 mm, excluding any stones, to prepare them for WDC analysis. WDC extraction followed a commonly used procedure, as described by Séquaris and Lewandowski (2003). In brief, approximately 10 g of soil was mixed with 20 ml of Milli-Q water (1:2) and shaken on a horizontal shaker at 150 rpm for 6 h. An additional 60 ml of deionized water was then added to the suspension, followed by a settling period. We calculated a sedimentation time of 10 min to remove particles larger than 20 μm according to Stokes' law. The supernatant, containing the non-settling phase, was carefully transferred into centrifugation tubes using a pipette. To isolate the desired colloids with a size smaller than 300 nm, centrifugation was carried out for 10 min at a speed of 7500 rpm (Biofuge, Heraeus, Hanau, Germany). The

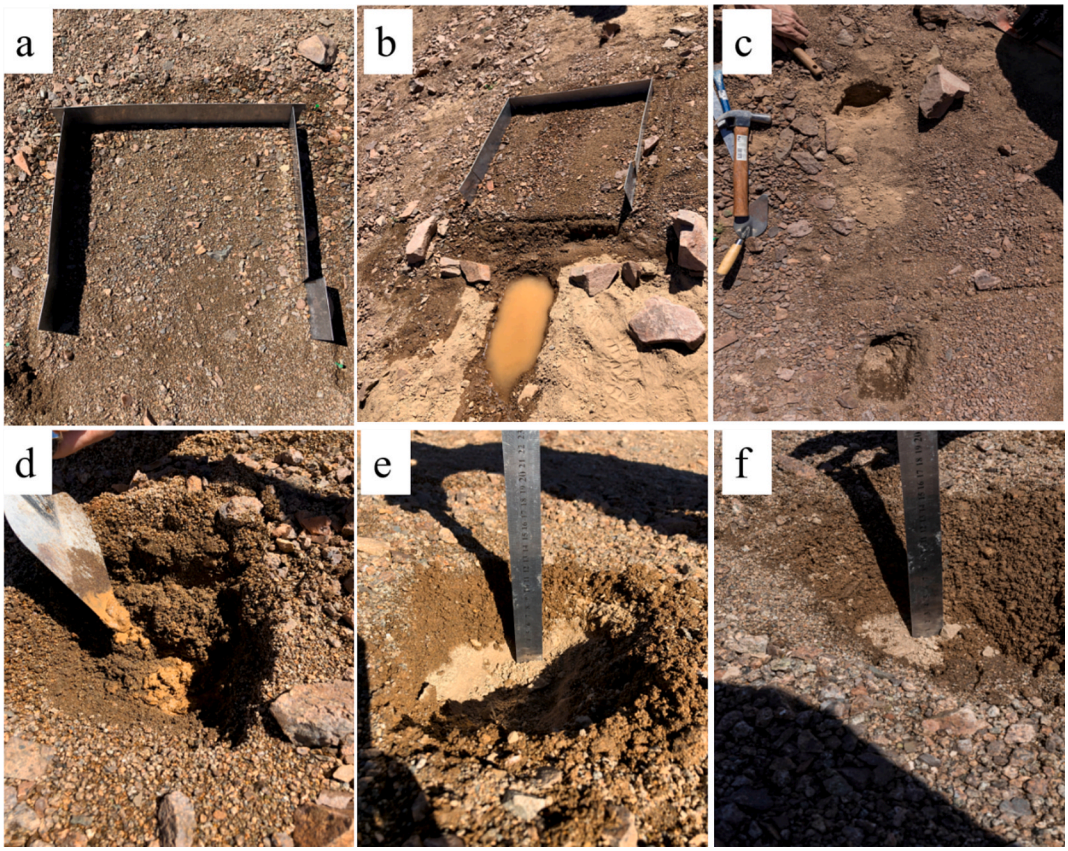

Fig. 3. Irrigation sampling (a) Pre-irrigation photos of the irrigated surface. (b) Post-irrigation photos of the irrigated surface. (c) Sampling sites 30 min after the irrigation experiment. The upper site is the control site, and the downward site is the irrigated site. (d–e) Sampling profiles of irrigated sites in the older fan section. Irrigation water permeated down to 10–15 cm below surface. (f) Sampling profile of an irrigated site in the younger fan section.

centrifugation time was determined according to the methodology described by Hathaway (1956). Dynamic light scattering (DLS) (Nano ZetaSizer, Malvern) measurements were then conducted to control the size range of the separated WDCs (Zhang et al., 2021).

2.5. Asymmetric flow field-flow fractionation (AF4)

The WDCs with sizes below 300 nm were fractionated using asymmetric flow field-flow fractionation (AF4) (AF2000, Postnova Analytics, Landsberg, Germany). To determine the WDC-OC content, the AF4 was coupled online with organic carbon detection (OCD; DOC-Labor, Karlsruhe, Germany). Furthermore, the concentrations of colloidal Mg, Al, Si, P, Ca, and Fe were measured using online inductively coupled plasma mass spectrometry (ICP-MS; Agilent 7500, Agilent Technologies, US). The parameters of the AF4 separation method were applied (Table S1), based on the study conducted by Moradi et al. (2020). The particle size resolution of the AF4 system was validated using sulfate latex (Postnova Analytics) analyzed under the same conditions as the samples, allowing for the conversion of elution time to colloid size (Moradi et al., 2020). In the Atacama Desert, three peaks of WDC size fractions can be determined: The first peak in the fractogram corresponded to nanocolloids (NCs) with a size range of 0.6–24 nm, while the second peak represented fine colloids (FCs) ranging from 24 nm to 210 nm. The medium colloids (MCs), eluting between 210 nm and 300 nm, constituted the third peak (Sun et al., 2023).

Quantification via ICP-MS and OCD was performed using external multipoint calibration (8 levels) and linear regression. Peak areas from the elution profiles were integrated and converted to concentrations (μM), which were then normalized to μmol WDC ions g^{-1} dry soil based on sample weight and moisture content. WDC content (OC, Mg, Al, Si, Ca, and Fe) was expressed as mg WDC ions per kg soil. As these elements represent the major components of WDCs, their sum was used as a proxy for total WDC content (Missong et al., 2018a; Moradi et al., 2020). Due to the low P concentrations, P content in the WDC fractions (WDC-P) was reported in μg WDC-P kg^{-1} of dry soil.

2.6. Statistical analysis

We assessed splash erosion by analyzing colloids in the 0–1 cm layer and identified particle leaching in the depth profile ranging from 1–15 cm, which was calculated by adding up the sub-layer values (1–5 cm, 5–10 cm, and 10–15 cm) using the following formula:

$$Cpro = \frac{(C1 \times 4 + C2 \times 5 + C3 \times 5)}{15} \quad (1)$$

C_{pro} (mg kg^{-1}) represents the content of the entire sampling sub-layer, which ranges from 1 cm to 15 cm for all sites except for the I3 site. C_1, C_2, and C_3 refer to the content of elements in the 1–5 cm, 5–10 cm, and 10–15 cm layers, respectively. For the I3 site, the depth profile referred to the 1–5 cm layer.

In this study, two fixed factors were considered: the formation age of the alluvial fan and the irrigation. Although a full-factorial design was originally planned to assess the effects of these two factors on soil aggregate fractions, MWD, WDCs content and the proportion of the sub-fractions, the relative proportions of elements in WDCs and their sub-fractions, as well as WDC-P distribution, large data variation and the nested structure of the sampling led us to adopt a more robust statistical approach. Specifically, linear mixed-effects models were employed to account for the fixed effects (fan age and irrigation) while incorporating sampling site as a random effect to address spatial dependency and improve the reliability of statistical inference. Pearson correlations were employed to examine: (1) the relationships between WDC, NC, FC, and MC content and soil aggregates fractions and MWD; and (2) the associations between WDC-P and the elements OC, P, Mg, Si, Al, Ca, and Fe in WDCs of three different size sub-fractions. All statistical analyses were performed using SPSS v22.0 (IBM, USA), and visualizations were created using OriginPro v9.1 (OriginLab, USA).

3. Results

3.1. The soil aggregate size distribution affected by irrigation

The irrigation effect on soil aggregate fractions varied across different soil depths (Table 1). In the surface layer (0–1 cm), irrigation significantly decreased macroaggregates (0.25–0.2 mm) along with an significant increasing microaggregates (0.053–0.25 mm). In the subsurface layer (>1 cm), the irrigation response was influenced by fan age. In the older fan section, macroaggregates decreased and microaggregates increased following irrigation. In contrast, the younger fan section showed increases in both macro- and microaggregate fractions post-irrigation (Table 1).

3.2. Size fractions and elemental composition of WDCs in the surface soil layer (0–1 cm)

FCs were the predominant particle size fraction of WDCs (65 ± 25 %) in the surface layer (0–1 cm) of the older fan section, whereas MCs accounted for a larger portion in the younger fan section (71 ± 10 %) before irrigation (Figs. 4, 5, 7b). After irrigation, FCs accounted for 35 ± 20 % and MCs became the predominant fraction (62 ± 20 %) in the older fan section. However, in the younger fan section, the percentage of MCs decreased to 52 ± 25 % and FCs increased from 21 ± 12 % to 44 ± 27 % (Fig. 7b).

To estimate the colloid content of the soils, the sum of the

Table 1
Effects of irrigation and sediment age on proportion of soil aggregate fractions (%) and mean weight diameter (MWD, mm).

Depth	Sites	>0.25 mm	>0.053 mm	>0.02 mm	<0.02 mm	MWD (mm)
0–1 cm	OL + T0[†]	85.2 ± 13.7[§]	13.3 ± 12.7	1.2 ± 1.1	0.3 ± 0.2	0.98 ± 0.1
	OL + T1	95.0 ± 5.3	4.2 ± 4.8	0.6 ± 0.6	0.2 ± 0.2	1.08 ± 0.05
	YO + T0	85.9 ± 12.0	12.3 ± 10.5	1.6 ± 1.4	0.2 ± 0.2	0.99 ± 0.1
	YO + T1	75.4 ± 11.4	23.6 ± 11.6	1.0 ± 0.3	0.2 ± 0.1	0.88 ± 0.1
>1 cm	OL + T0	62.4 ± 3.8	35.4 ± 4.4	0.8 ± 0.5	1.4 ± 1.7	0.76 ± 0.04
	OL + T1	56.8 ± 12.7	41.4 ± 12.3	1.2 ± 0.6	0.6 ± 0.2	0.70 ± 0.1
	YO + T0	68.1 ± 10.4	29.5 ± 9.6	2.1 ± 1.0	0.3 ± 0.03	0.81 ± 0.1
	YO + T1	68.7 ± 13.5	29.7 ± 12.4	1.1 ± 0.8	0.6 ± 0.5	0.82 ± 0.1
Analysis of variance (P values) for parameters as affected by sediment age and irrigation						
0–1	Age	NS	NS	NS	NS	NS
	Irrigation	0.011*	0.008*	NS	NS	NS
	Age × Irrigation	NS	NS	NS	NS	NS
>1	Age	NS	NS	NS	NS	NS
	Irrigation	0.008*	0.008*	NS	NS	NS
	Age × Irrigation	0.041*	0.036*	NS	NS	NS

*Indicates significant at $p < 0.05$, **indicates significant at $p < 0.001$.

[†] OL = sites on the older fan section, including I1, I2 and I3, YO = sites on the younger fan section, including I4, I5, and I6. T0: before irrigation; T1: at the end of 30 min of irrigation.

[§] The value was given as mean ± SD, n = 3.

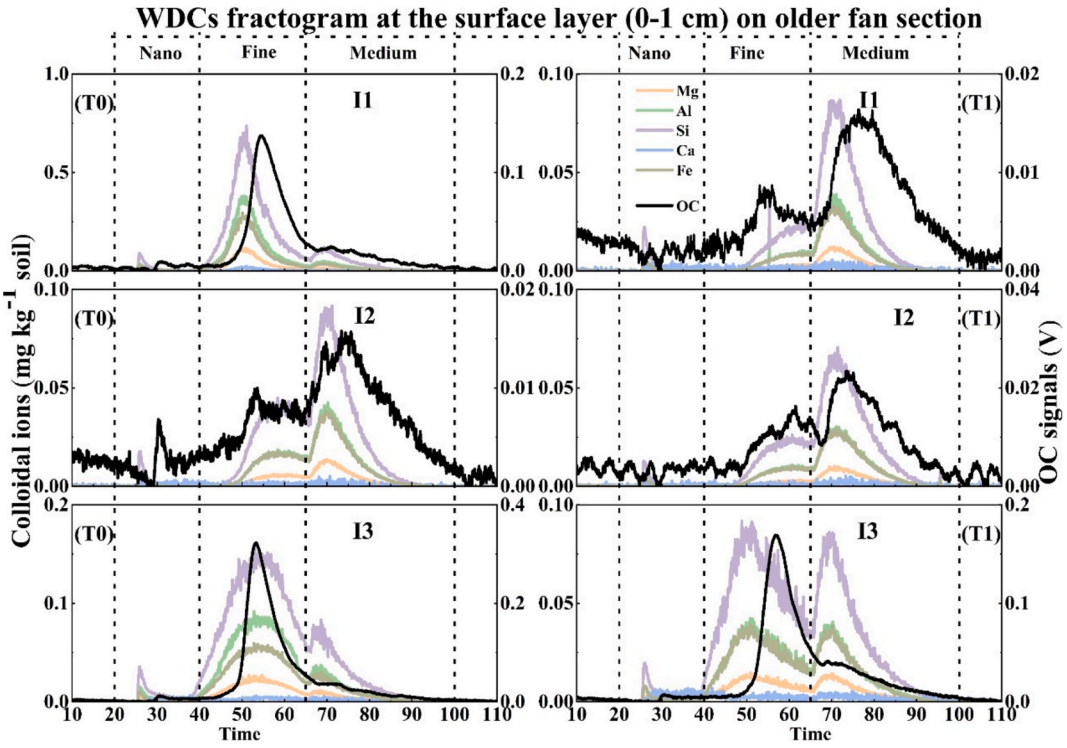

Fig. 4. Fractogram of water-dispersible colloid (WDC) elements, e.g., magnesium (Mg), aluminum (Al), silicon (Si), calcium (Ca), iron (Fe), and organic carbon (OC) of the top layer (0–1 cm) at sites (including sites I1, I2, I3) on the older fan section, obtained by flow field-flow fractionation (FFF) coupled with inductively coupled plasma mass spectrometry (ICP-MS) and organic carbon detection (OCD). T0: before irrigation; T1: at the end of 30 min of irrigation. Nano: Nanocolloid fraction from 0.6 nm to 24 nm; Fine: Fine colloid fraction from 24 nm to 210 nm; Medium: Medium colloid fraction from 210 nm to 300 nm. Note different scaling of Y-axes for the 6 figures. Axis ranges differ among the six panels to enhance visibility of trends. All panels use the same measurement units and indicators for direct comparison.

concentrations of seven colloidal elements (OC, P, Mg, Al, Si, Ca, Fe) was used as a proxy, where Si, Al, and Fe were the predominant elements in the WDCs and their sub-fractions across both sections (Table S3). In the surface layer (0–1 cm) of the older fan section pre-irrigation, the WDC content amounted to 154 ± 117 mg kg^{-1}, while a relatively lower concentration of WDCs (37 ± 19 mg kg^{-1}) was found in the younger fan section (Fig. 7a). Interestingly, they exhibited the opposite response to irrigation (Fig. 7a). The WDC content decreased to 58 ± 29 mg kg^{-1} in the older fan section and increased to 87 ± 78 mg kg^{-1} in the younger fan section (Fig. 7a).

3.3. Size fractions and elemental composition of WDCs in the subsurface soil layer (>1 cm)

In the >1 cm soil layer post-irrigation, changes in the content of WDCs and sub-fractions were observed (Fig. 7c). The WDC content increased from 130 ± 120 to 261 ± 106 mg kg^{-1} in the older fan section (Fig. 7), while a declining trend was observed in the younger fan section, decreasing from 111 ± 65 mg kg^{-1} to 95 ± 27 mg kg^{-1} (Fig. 7c). Without irrigation, FCs dominated the WDCs, constituting 63 ± 17 % in the younger fan section and 64 ± 9 % in the older fan section (Fig. 7d). Interestingly, irrigation increased the proportion of FCs in the older fan section to 75 ± 8 %, while it slightly decreased to 61 ± 13 % in the younger fan section (Fig. 7d). These variations were not significant (Table S3).

Although both irrigation and fan age showed limited effect on the relative proportion of the elemental composition of WDCs and their sub-fractions, Si, Al and Fe were the predominant elements in the WDCs and their sub-fractions for all sites (Table S4).

3.4. Phosphorus associated with WDCs

In general, the variation of the colloidal-P content and fractions was comparable to the variations of the WDCs (Figs. 4, 5 and 6). In the surface layer (0–1 cm), a decrease in the water-dispersible colloidal phosphorus (WDC-P) content from 394 ± 395 μg kg^{-1} to 208 ± 48 μg kg^{-1} was observed after irrigation at sites in the older fan section (Fig. 8a). Conversely, sites located in the younger fan section exhibited a notable increase in WDC-P content from 124 ± 55 μg kg^{-1} to 324 ± 209 μg kg^{-1} (Fig. 8a). In the subsurface layer (>1 cm), sites situated in the younger fan section displayed a slight decrease from 613 ± 284 μg kg^{-1} to 542 ± 324 μg kg^{-1} (Fig. 8b), while sites in the older fan section showed an increase from 260 ± 313 μg kg^{-1} to 542 ± 324 μg kg^{-1} WDC-P (Fig. 8b).

Three sub-fractions (NC-P, FC-P, and MC-P) were observed in the surface layer (0–1 cm) (Fig. 6). Before irrigation, FC-P was the dominant fraction in the older fan section (62 ± 22 %), and MC-P was the primary one in the younger fan section (45 ± 7 %) (Fig. 6, Fig. 8b). Interestingly, irrigation significantly increased NC-P from 8 ± 5 % to 23 ± 6 % in the younger fan section (Fig. 8). In the subsurface layer (>1 cm), FC-P was predominant in the WDCs for all sites. Furthermore, the fractions of MC-P decreased notably from 35 ± 10 % to 16 ± 5 % in the older fan section after irrigation.

Correlation analysis revealed that WDC-P showed a significant dependence on colloidal mineral elements, including Fe, Al, Mg, Si, and OC. In the sub-fractions, FC-P exhibited a positive relationship with all mineral elements and OC (Table S5).

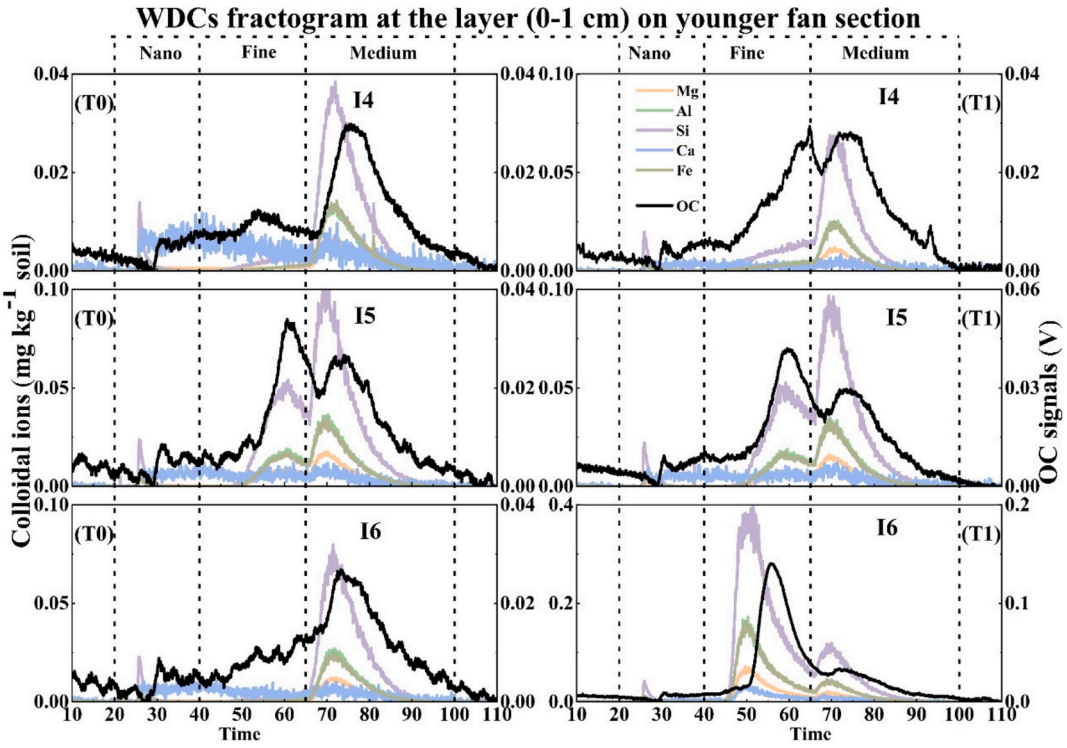

Fig. 5. Fractogram of water-dispersible colloid (WDC) elements, e.g., magnesium (Mg), aluminum (Al), silicon (Si), calcium (Ca), iron (Fe), and organic carbon (OC) of the top layer (0–1 cm) at sites (including sites I4, I5, I6) on the younger fan section, obtained by flow field-flow fractionation (FFF) coupled with inductively coupled plasma mass spectrometry (ICP-MS) and organic carbon detection (OCD). T0: before irrigation; T1: at the end of 30 min of irrigation. Nano: = Nanocolloid fraction from 0.6 nm to 24 nm; Fine: = Fine colloid fraction from 24 nm to 210 nm; Medium: = Medium colloid fraction from 210 nm to 300 nm. Note different scaling of Y-axes for the 6 figures. Axis ranges differ among the six panels to enhance visibility of trends. All panels use the same measurement units and indicators for direct comparison.

4. Discussion

4.1. Water movement and potential particle transport following irrigation

The infiltration rates in desert soils gradually decline with age (Greenbaum et al., 2020) accompanied by a reduction of surface roughness and the formation of a flat, smooth, and well-developed desert pavement (Houston, 2002; Meadows et al., 2008), as shown in our older fan section (Table S2; Sun et al., 2023). However, infiltration capacity in both the younger (~14 ka, 244 mm h^{-1}) and older (~56 ka, ~181 mm h^{-1}) fan sections remains far above the applied irrigation rate of 44.8 mm h^{-1} (Pfeiffer et al., 2021; Sun et al., 2023), suggesting that water would predominantly infiltrate rather than generate surface runoff. Consistent with this, no surface runoff or visible sediment transport was observed despite a steel chute was installed to capture potential runoff (Fig. 2A). Instead, subsurface flow emerged ~10 min after irrigation (Fig. 3b), with water infiltrating vertically to ~15 cm depth before moving laterally downslope (Fig. 3b, d and e), consistent with previous studies (Arens et al., 2021; Owen et al., 2013; Pfeiffer et al., 2021). While evaporation has a strong impact in the Atacama Desert (Houston, 2006a), its immediate effect on infiltration-driven water movement appears limited. Pfeiffer et al. (2021) reported a persistent downward flux of vapor lasting over half a month after rainfall and May et al. (2020) observed moisture migration to ~25 cm depth for three days post-irrigation. In our study, short-term water redistribution was driven by infiltration and downslope subsurface flow. These processes directly influence the mobility and fate of soil particles, especially fine particles such as WDCs that are more easily mobilized under specific hydrological conditions (Martínez-Mena et al., 2002). In turn, the presence and movement of fine particles can affect soil porosity and hydraulic conductivity, modifying water flow patterns over time (Moradi et al., 2020).

4.2. Effects of irrigation and sediment age on the elemental composition of WDCs

The content of WDCs (<300 nm) and fine soil particles (<0.25 mm) showed greater spatial variation across sites—despite having similar sediment age and undergoing the same irrigation treatment—than that of coarser particles (>0.25 mm), with standard deviations in some sites comparable to the mean values (Table 1, Table S3). This high heterogeneity suggests that fine soil fractions are more sensitive to local environmental disturbances such as micro-relief, plant distribution, and aerosol deposition (Moradi et al., 2020; Sun et al., 2023). Although our results did not show a clear trend of increased heterogeneity with increasing sediment age, previous studies have suggested that long-term pedogenesis can intensify spatial variability (Huang et al., 2016), particularly in arid environments where soil development is strongly time-dependent (Delgado-Baquerizo et al., 2020). Nevertheless, our results, supported by statistical analysis, revealed that sediment age significantly influenced the composition of WDCs in alluvial fan sites (Table S4, Table S5), especially in the nano-colloids (NCs). In line with the findings of Sun et al. (2023), the older fan surface (0–1 cm) exhibited a lower proportion of NCs (Table S3) and a distinct elemental profile, characterized by less Ca and more Al and Fe in both WDCs and NCs (Figs. 3, 4, Table S4). These trends are consistent with age-driven patterns of decalcification and initial rubification during early pedogenesis in the desert environment (Ebeling et al., 2016; Walk et al., 2023).

Although irrigation showed limited effect independently on the elemental composition (Al, Si, Ca) of surface NCs, its significant interaction with sediment age ($p < 0.05$; Table S4) suggests that short-term disturbance-such as irrigation or extreme rainfall events-can mitigate age-driven differences in the proportions of NC-Al, NC-Si, and NC-Ca. These effects are likely associated with enhanced chemical dissolution or increased NCs mobility induced by leaching. Notably, a significant

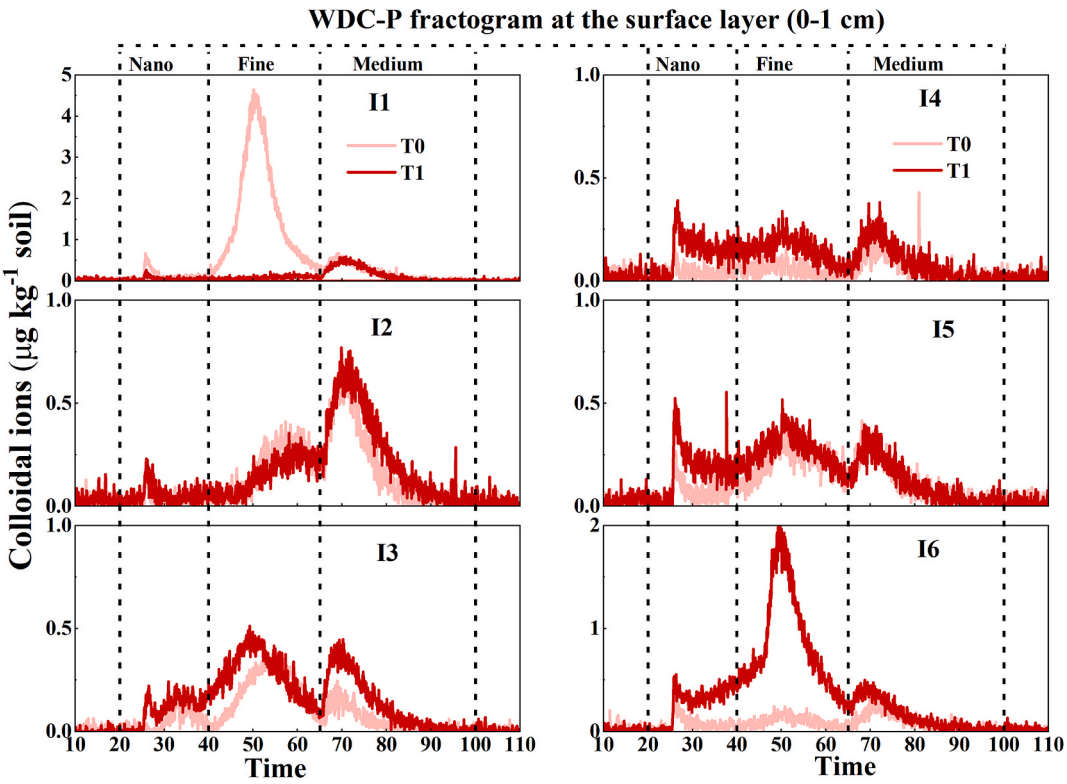

Fig. 6. Fractogram of nanocolloidal (Nano), fine-colloidal (Fine), and medium-colloidal (Medium) phosphorus (P) at the surface layer (0–1 cm) analyzed by asymmetrical flow field-flow fractionation (AF4) coupled with inductively coupled plasma mass spectrometry (ICP-MS). I1, I2 and I3 belong to the older fan section, I4, I5, and I6 are in the younger fan section. T0: before irrigation; T1: at the end of 30 min of irrigation. Axis ranges differ among the six panels to enhance visibility of trends. All panels use the same measurement units and indicators for direct comparison.

interaction between irrigation and sediment age was also observed for the Si/Al ratio in surface WDCs (Table S4). The Si/Al ratio, which was over 2, may be related to multiple sources of WDCs, including mineral assemblages and sand-derived particles (Moradi et al., 2020; Sun et al., 2023). Anorthite, with a Si/Al ratio of 1:1, and albite, with a Si/Al ratio of 3, are the dominant components of atmospheric dust deposition near the study site (Wang et al., 2014). Additionally, sand-derived particles, which contribute more silicon, also enhance the Si/Al ratio in WDCs (Moradi et al., 2020). Consistent with Sun et al. (2023), age tended to reduce the Si/Al ratio (Table S4), which may reflect selective loss of Si-enriched components or increased Al input through weathering (He et al., 2008).

4.3. Potential mechanisms driving WDCs dynamics following irrigation

Although irrigation did not cause statistically significant changes in WDC content, observable trends suggest a dynamic response (Table S3, Fig. 7). This lack of significance is likely due to the interplay of multiple mechanisms: (1) the loss of WDCs via water movement as discussed in section 4.1 or soil aggregation and (2) the release of WDCs by aggregate disintegration. This is supported by the negative correlation between MWD and WDC content (Table S6), indicating that lower MWD—reflecting weaker structural stability—was associated with greater WDC release. A higher MWD, in contrast, typically reflects stronger resistance to external forces and limits colloid mobilization (Hu et al., 2023). These opposing processes may offset each other, resulting in no net detectable change in fine particles, especially WDCs, at the statistical level. In contrast to WDCs, larger soil aggregates (>0.053 mm) have been shown to respond more readily to short-term hydrological events (Table 1; Dal Ferro et al., 2023; Shi et al., 2017), highlighting the relatively stable or buffered nature of colloidal particles. Consequently, WDCs have often been overlooked in past analyses. We therefore conducted further analysis of these trends to identify the dominant processes influencing WDC dynamics during irrigation, which appear to be governed by soil texture and age-related differences in aggregation.

4.3.1. Irrigation effect on WDCs in the soil of younger fan section

In the surface layer (0–1 cm) of the younger fan section, the content of WDCs increased due to irrigation (Figs. 5 and 7) and there was a decrease in macroaggregates (0.25–2 mm) and a rise in microaggregates (0.053–0.25 mm) (Table 1). Simultaneously, the proportion of FCs increased while that of MCs decreased (Figs. 5 and 7). This means that the disintegration of soil particles drove the release of fine particles. The process was likely driven by the impact of raindrops and runoff transport (Fernández-Raga et al., 2017; Li et al., 2018; Lv et al., 2023; Meshesha et al., 2016). Both raindrop kinetic energy and soil internal forces affect splash erosion (Ghahramani et al., 2012; Liu et al., 2021). The breakdown of soil aggregates by splash erosion was facilitated by the weak cohesive forces due to the low clay content (1 %, Fig. S2). Despite the rainfall simulator provided less kinetic energy than natural rainfall (Iserloh et al., 2013), raindrop energy ($\sim 3.7 \times 10^{-4}$ J) was sufficient to disperse soil aggregates (Li et al., 2018; Zambon et al., 2021), especially in the top centimeter of soil (Lv et al., 2023).

In the subsurface (>1 cm), the initial WDC content was larger than that in the surface layer (Fig. 5, Fig. 7), consistent with leaching accumulation (Moradi et al., 2020). After irrigation, WDC content decreased by nearly 14 % alongside increased macro- and microaggregates (Table 1), rising MCs and a decrease in FCs (Fig. 7), suggesting that aggregation processes may have been induced. Soil aggregation may occur during the drainage and drying period (Mohanty et al., 2015; Wang et al., 2020a). Studies have shown that if the duration of drying exceeds a threshold, salts or minerals in the evaporating pore water can precipitate and bind the fine particles like colloids rather than release them (Mohanty et al., 2015; van den Bogaert et al., 2016). A closer

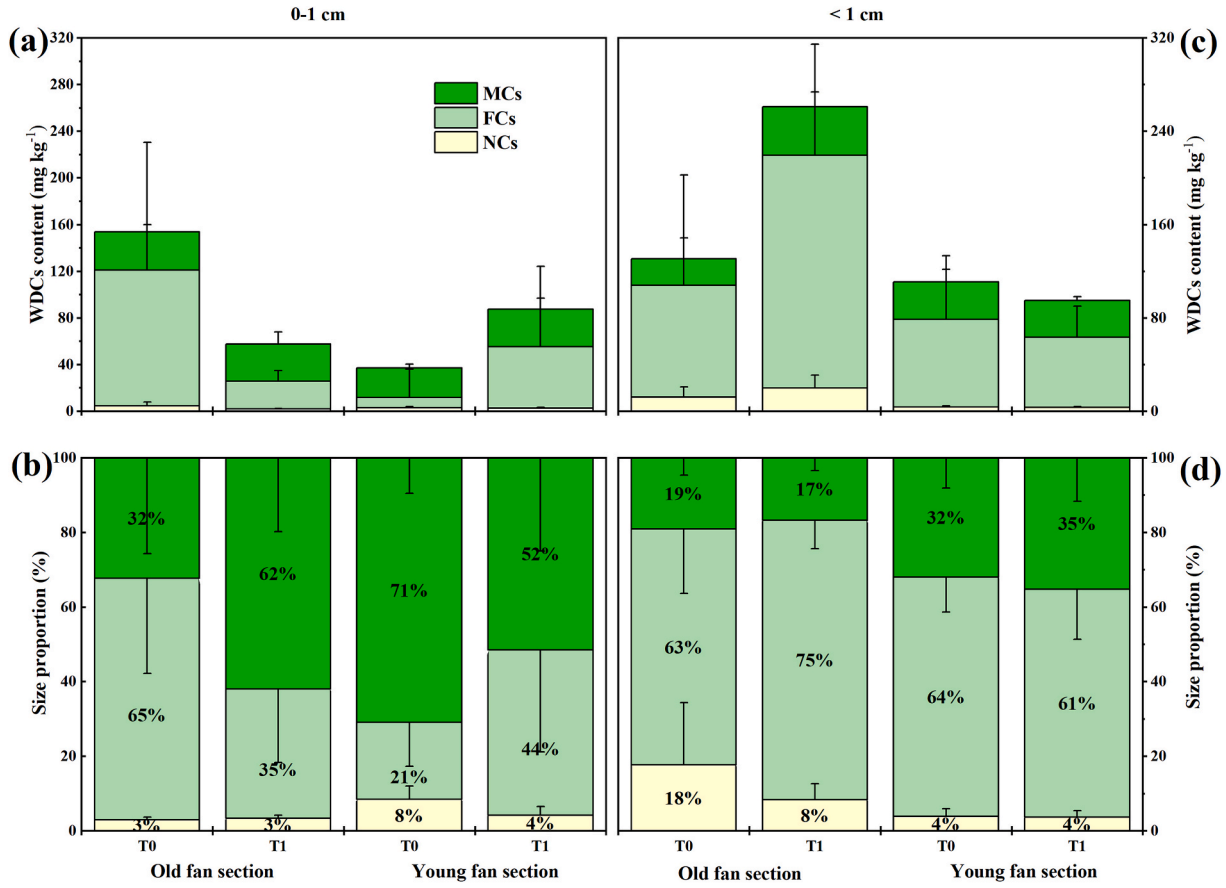

Fig. 7. (a) Element concentrations of WDCs (OC, Mg, Al, Si, Ca, and Fe) in the surface layer (0–1 cm) of the alluvial fan; total WDC content was calculated as their sum, expressed in mg g^{-1} dry soil. (b) Proportions of 3 size fractions for WDCs in the surface layer (0–1 cm) of the alluvial fan. (c) Element concentrations of WDCs (OC, Mg, Al, Si, Ca, and Fe) in the subsurface layer (>1 cm) of the alluvial fan; total WDC content was calculated as their sum, expressed in mg g^{-1} dry soil. (b) Proportions of 3 size fractions for WDCs in the subsurface layer (>1 cm) of the alluvial fan. I1, I2 and I3 belong to the older fan section, I4, I5, and I6 are in the younger fan section. T0: before irrigation; T1: at the end of 30 min of irrigation.

approach distance for the colloids following a decrease in the soil water content may initiate cementation processes (Majdalani et al., 2008). Sampling conducted after 30 min of irrigation may have captured early aggregation effects. Additionally, WDCs loss may stem from downslope subsurface flow (Fig. 2), a process prominent under conditions of high infiltration rate and soil permeability (El-farhan et al., 2000; Zhang et al., 2016). Similar downward colloid accumulation was observed in this fan system by Moradi et al. (2020) and Sun et al. (2023).

4.3.2. *Irrigation effect on WDCs in the soil of the older fan section*

By contrast to the younger fan section, opposite WDC dynamics were observed in the older fan section following irrigation (Fig. 7). In the topsoil (0–1 cm), there was a decrease in WDCs with NCs and FCs decreasing by 57 % and 80 %, respectively, and MCs slightly declining (Fig. 7).This implies that colloid transport dominated over disintegration. It appears that the kinetic energy of raindrops or irrigation water droplets did not exceed soil strength (Auerswald, 1995; Blanco-Moure et al., 2012; Shi et al., 2012; Xiao et al., 2017). In general, the clay content helps to increase the mineral surface area of aggregates and enhances the cohesive strength of the soil (Almajmaie et al., 2017; Hu et al., 2018; Ma et al., 2022; Schweizer et al., 2019; Totsche et al., 2018; Zambon et al., 2021). Therefore, the increased clay content (7 %, Table S2) in the older surface layer (0–10 cm) reduced the mechanical breakdown and thus soil erodibility by raindrops (Ayoubi et al., 2022; Lebissonnais, 2016) or irrigation water droplets. The hard surface described by Moradi et al. (2020) as a 'crust' may have further minimized splash erosion.

In the deeper layer (>1 cm), WDCs showed a one-fold increase post-irrigation (Fig. 7). This can likely be attributed to colloid leaching from the surface layer. The presence of a solid mineral layer (Sun et al., 2023) may inhibit deeper transport, facilitating colloid accumulation in the 5–10 cm depth. Furthermore, the increased WDCs content was associated with aggregate disintegration within the layer. The reduction in macroaggregates (0.25–2 mm) along with the increase in microaggregates (0.053–0.25 mm) and the increase in the proportion of FCs along with the decrease of MCs further indicate a disintegration process (Table 1). In the deeper layer (>1 cm), the disintegration of soil aggregates is mainly induced by swelling and clay dispersion, with raindrop impact playing an insignificant role (Tanner et al., 2021; Torkzaban et al., 2015; Vaezi et al., 2017). The increased clay content (7 %) compared with that of the younger fan section can lead to increased swelling when wet, potentially causing further aggregate breakdown (Hu et al., 2015; Lebissonnais, 2016). These findings are consistent with previous reports of subsurface WDC enrichment in the older fan section (Sun et al., 2023).

4.4. *Irrigation effect on WDC-P in soil layers*

The response of overall WDC-P to irrigation displayed a consistent and simultaneous trend with WDCs (Figs. 6, 7 and 8). Specifically, WDC-P exhibited a decrease in the surface layer (0–1 cm), while showing an increase in the subsurface layer (>1 cm) in the older fan section. Conversely, in the younger fan section, the opposite trend was observed (Fig. 8). A positive correlation between WDC-P and colloidal elements

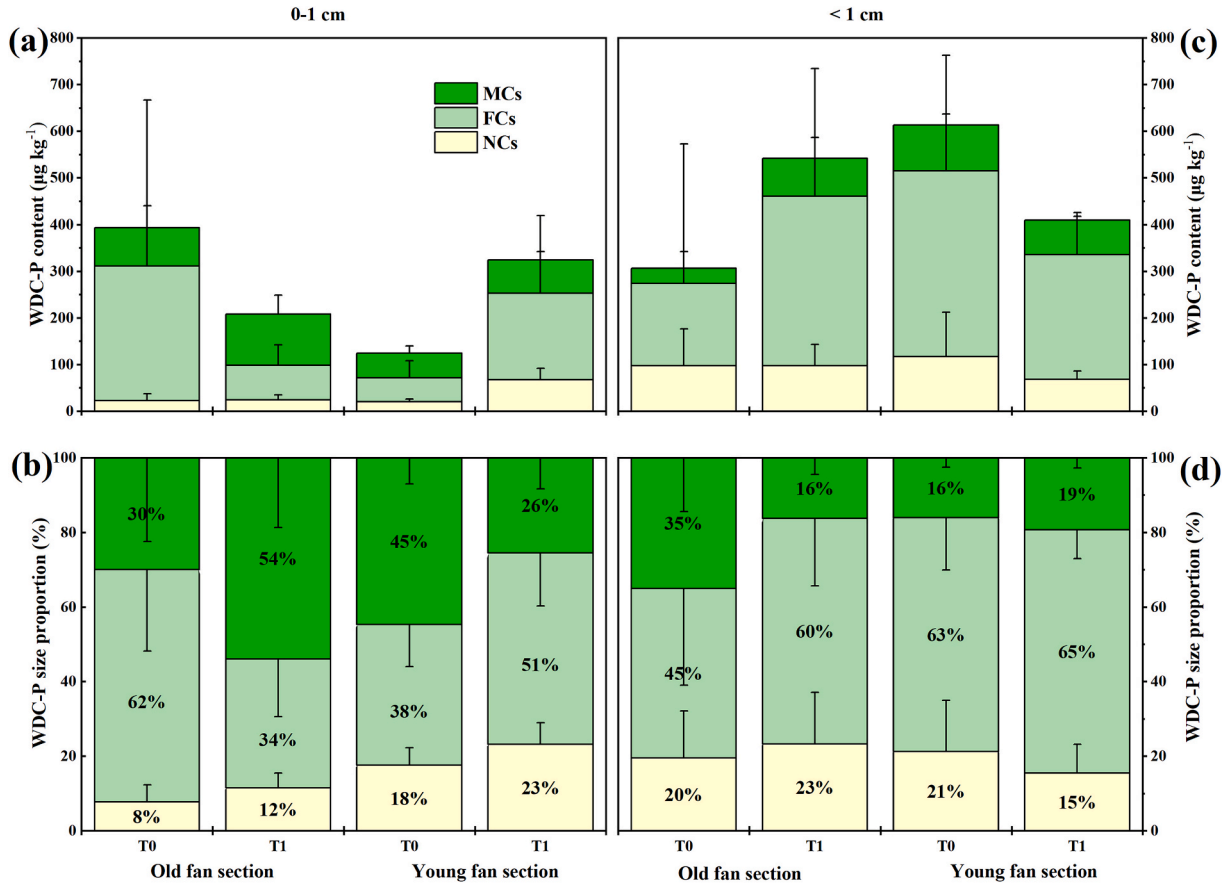

Fig. 8. (a) Element concentrations of WDC-P in the surface layer (0–1 cm) of the alluvial fan. (b) Proportions of 3 size fractions for WDC-P in the surface layer (0–1 cm) of the alluvial fan. (c) Element concentrations of WDC-P in the subsurface layer (>1 cm) of the alluvial fan. (b) Proportions of 3 size fractions for WDC-P in the subsurface layer (>1 cm) of the alluvial fan. I1, I2 and I3 belong to the older fan section, I4, I5, and I6 are in the younger fan section. T0: before irrigation; T1: at the end of 30 min of irrigation.

(Si, Al, Fe, Mg, and OC; Table S7) supports that WDC-P is influenced by the elemental composition of WDCs (Jiang et al., 2023; Sun et al., 2023; Zhang et al., 2023), which in turn shifted with irrigation (Table S4, Table S5). As phyllosilicate clay minerals and Fe/Al-(hydr)oxides are colloidal sources and P sorbents (Kahle et al., 2004; Wang et al., 2021b; Zhang et al., 2021) in the study area, their dynamics affected the redistribution of WDC-P.

However, in some cases following irrigation, variations of P associated with colloidal sub-fractions (NCs, FCs, and MCs) were observed to be not in accordance with those of the sub-fractions (Figs. 7 and 8). NCs accounted for 3–18 % of WDCs, and there was a decrease of NCs in the younger surface layer with increasing WDCs after irrigation (Fig. 7). This may be related to the fact that nanoparticles were susceptible to being transported with irrigation water droplets. However, the proportion of NC-P accounted for 8–23 % of WDC-P and irrigation led to a remarkable three-fold rise in NC-P in the younger surface soil (Fig. 8). Correlation analysis revealed that NC-P correlated with major mineral elements (Si, Al, Mg, Fe) in NCs, but showed no relationship with NC-Ca (Table S7). Moradi et al. (2020) reported that Ca readily retained P by forming insoluble Ca-P salts, and Ca^{2+} may function as a cation bridge to form complexes such as OC-Ca-P. However, the relatively low concentration of NC-OC restricted the role of Ca in the formation of NC-P (Fig. 6). In the younger surface layer, instead of NC-Ca, the presence of NC-Si and NC-Al as likely clay minerals and Al (hydr)oxides may increase the content of NC-P in this size fraction (Table S4). Therefore, changes in WDC-P in response to irrigation are controlled not only by the quantity of NCs but also by their elemental composition.

FC-P comprised the majority of WDCs (34–65 %) and varied in accordance with FCs (Figs. 7 and 8). Consistent with the previous study (Sun et al., 2023), FC-P correlated with both OC and mineral elements, even Ca (Table S6). Ca was able to form complexes of OC-Ca-P in the fractions of both FCs and MCs (Wang et al., 2020b; Zhang et al., 2023). However, in our study, MC-P, which changed along with WDCs, showed no correlation with MC-OC. It has also been observed in previous studies that OC plays a minor role in associating P in MCs in the hyper-arid soils (Moradi et al., 2020; Sun et al., 2023).

5. Conclusion

The Atacama Desert is one of the harshest environments for life on Earth. In this study, we investigated how intense rainfall events affect the behavior of water-dispersible colloids (WDCs) and their associated phosphorus (WDC-P) distribution in this hyper-arid region. Although irrigation did not cause statistically significant changes in the overall content or sub-fractions of WDCs, our results indicate that WDCs exist in a dynamic balance between aggregation/disintegration and transport processes. These dominant processes varied with soil depth and sediment age, likely driven by differences in clay content and soil structure shaped by pedogenic development. Notably, even a short-term irrigation event induced detectable changes in the elemental composition of WDCs. This, in turn, altered WDC-P behavior, particularly within the nano-colloid sub-fraction (0.6–24 nm), where the associated elemental constituents changed. Our findings highlight that, although rainfall events are rare in hyper-arid environments, their influence on nutrient cycling and landform evolution is not negligible. While our study captured the effects of a single rainfall event, the cumulative impact of

such hydrological disturbances over millennia could be profound, especially regarding colloid-mediated processes. However, the absence of water sample collection in this study limited our ability to quantitatively assess colloid transport and loss. Future studies should incorporate water-phase analysis and longer-term monitoring to validate the persistence and broader implications of the observed trends.

CRediT authorship contribution statement

Xiaolei Sun: Writing – review & editing, Writing – original draft, Methodology, Investigation, Formal analysis, Data curation. **Simon Matthias May:** Writing – review & editing, Investigation. **Alain Mollier:** Writing – review & editing, Data curation. **Miaoyue Zhang:** Writing – review & editing, Methodology, Funding acquisition. **Qian Zhang:** Writing – review & editing, Methodology. **Bárbara Fuentes:** Writing – review & editing, Investigation, Data curation. **Franko Arenas:** Investigation, Data curation. **Roland Bol:** Writing – review & editing, Project administration, Methodology, Investigation, Conceptualization. **Erwin Klumpp:** Writing – review & editing, Supervision, Project administration, Methodology, Funding acquisition, Conceptualization.

Declaration of competing interest

The authors declare that they have no known competing financial interests or personal relationships that could have appeared to influence the work reported in this paper.

Acknowledgements

This work was conducted as part of a Collaborative Research Centre project: “Earth - Evolution at the Dry Limit,” which was funded by the German Research Foundation (DFG), project no. 268236062–SFB 1211. Miaoyue Zhang and Roland Bol are grateful for the support of the Sino–German project M-0749. Xiaolei Sun would like to thank the China Scholarship Council (CSC:201904910544) for supporting her study at RWTH Aachen University and Forschungszentrum Jülich. The authors would like to thank Anael Videla and Francisco Gomez for sampling. The pictures in Fig. 3 were kindly provided by Francisco Gomez. The authors would also like to thank Dr. Nina Siebers and Dr. Volker Nischwitz (ZEA-3, Forschungszentrum Jülich) for their support with the AF4 test.

Appendix A. Supplementary data

Supplementary data to this article can be found online at https://doi.org/10.1016/j.catena.2025.109355.

References

Almajmaie, A., Hardie, M., Acuna, T., Birch, C., 2017. Evaluation of methods for determining soil aggregate stability. Soil Tillage Res. 167, 39–45.
Arenas-Díaz, F., Fuentes, B., Reyers, M., Fiedler, S., Böhm, C., Campos, E., Shao, Y., Bol, R., 2022. Dust and aerosols in the Atacama Desert. Earth Sci. Rev. 226, 103925.
Arens, F.L., Airo, A., Feige, J., Sager, C., Wiechert, U., Schulze-Makuch, D., 2021. Geochemical proxies for water-soil interactions in the hyperarid Atacama Desert. Chile. Catena 206, 105531.
Artieda, O., Herrero, J., 2003. Pedogenesis in lutitic Cr horizons of gypsiferous soils. Soil Sci. Soc. Am. J. 67 (5), 1496–1506.
Auerswald, K., 1995. Percolation stability of aggregates from arable topsoils. Soil Sci. 159, 142–148.
Ayoubi, S., Milikian, A., Mosaddeghi, M.R., Zeraatpisheh, M., Zhao, S., 2022. Impacts of clay content and type on shear strength and splash erosion of clay-sand mixtures. Minerals 12, 1339.
Bach, E.M., Hofmockel, K.S., 2014. Soil aggregate isolation method affects measures of intra-aggregate extracellular enzyme activity. Soil Biol. Biochem. 69, 54–62.
Baken, S., Moens, C., Grift, B.V.D., Smolders, E., 2016a. Phosphate binding by natural iron-rich colloids in streams. Water Res. 98, 326–333.
Baken, S., Regelink, I.C., Comans, R.N.J., Smolders, E., Koopmans, G.F., 2016b. Iron-rich colloids as carrier of phosphorus in streams: a field-flow fractionation study. Water Res. 99, 83–90.
Blanco-Moure, N., Moret-Fernández, D., Victoria López, M., 2012. Dynamics of aggregate destabilization by water in soils under long-term conservation tillage in semiarid Spain. Catena 99, 34–41.
Bozkurt, D., Rondanelli, R., Garreaud, R., Arriagada, A., 2016. Impact of warmer eastern tropic Pacific SST on the March 2015 Atacama floods. Mon. Weather Rev. 144 (11), 4441–4460.
Cabré, A., Remy, D., Aguilar, G., Carretier, S., Riquelme, R., 2020. Mapping rainstorm erosion associated with an individual storm from InSAR coherence loss validated by field evidence for the Atacama Desert. Earth Surf. Proc. Land. 45 (9), 2091–2106.
Cerdà, A., 1997. Seasonal changes of the infiltration rates in a Mediterranean scrubland on limestone. 198 (1–4), 209–225.
Christiansen, 1942. Hydraulics of sprinkling systems for irrigation, 107(1).
Dal Ferro, N., Stevenson, B., Morari, F., Müller, K., 2023. Long-term tillage and irrigation effects on aggregation and soil organic carbon stabilization mechanisms. Geroderma 432, 116398.
Davis, W.L., Pater, I.D., McKay, C.P., 2009. Rain infiltration and crust formation in the extreme arid zone of the Atacama Desert, Chile. Planet. Space Sci. 58 (4), 616–622.
Delgado-Baquerizo, M., Reich, P.B., Bardgett, R.D., Eldridge, D.J., Lambres, H., Wardle, D.A., Reed, S.C., Plaza, C., Png, G.K., Neuhauser, S., Berhe, A.A., Hart, S.C., Hu, H., He, J., Bastida, F., Abades, S., Alfaro, F.D., Culter, N.A., Gallardo, A., García-Velázquez, L., Hayes, P.E., Hseu, Z.Y., Pérez, C.A., Santos, F., Siebe, C., Trivedi, P., Sullivan, B.W., Weber-Grullon, L., Williams, M.A., Fierer, N., 2020. The influence of soil age on ecosystem structure and function across biomes. Nat. Commun. 11, 4721.
Dunai, T.J., Melles, M., Quandt, D., Knief, C., Amelung, W., 2020. Whitepaper: earth – evolution at the dry limit. Global Planet. Change 193, 103275.
Ebeling, A., Oerter, E., Valley, J.W., Amundson, R., 2016. Relict soil evidence for profound quaternary aridification of the Atacama Desert, Chile. Geoderma 267, 196–206.
El-farhan, Y.H., Denovio, N.M., Herman, J.S., Hornberger, G.M., 2000. Mobilization and transport of soil particles during infiltration experiments in an agricultural field, Shenandoah Valley, Virgnia. Environ. Sci. Technol. 34 (17), 3555–3559.
Eshel, G., Araus, V., Undurraga, S., Soto, D.C., Moraga, C., Montecinos, A., Moyano, T., Maldonado, J., Díaz, F.P., Varala, K., Nelson, C.W., Contreras-López, O., Pal-Gabor, H., Kraiser, T., Carrasco-Puga, G., Nilo-Poyanco, R., Zegar, C.M., Orellana, A., Montecino, M., Maass, A., Allende, M.L., DeSalle, R., Stevenson, D.W., González, M., Latorre, C., Coruzzi, G., Gutiérrez, R.A., 2021. Plant ecological genomics at the limits of life in the Atacama Desert. PNAS 118 (46), e2101177118.
Ewing, S.A., Michalski, G., Thiemens, M., Quinn, R.C., Macalady, J.L., Kohl, S., Wankel, S.D., Kendall, C., McKay, C.P., Amundson, R., 2007. Rainfall limit of the N cycle on Earth. Global Biogeochem. Cycles 21 (3), GB3009.
Ewing, S.A., Sutter, B., Owen, J., Nishiizumi, K., Sharp, W., Cliff, S.S., Perry, K., Dietrich, W., McKay, C.P., Amundson, R., 2006. A threshold in soil formation at Earth’s arid-hyperarid transition. Geochim. Cosmochim. Acta 70, 5293–5322.
Fajardo, M., McBratney, A.B., Field, D.J., Minasny, B., 2016. Soil slaking assessment using image recognition. Soil Tillage Res. 163, 119–129.
Fernández-Rag, M., Palencia, C., Keesstra, S., Jordán, A., Fraile, R., Angulo-Martínez, M., Cerdà, A., 2017. Splash erosion: a review with unanswered questions. Earth Sci. Rev. 171, 463–477.
Fomin, D., Timofeeva, M., Ovchinnikova, O., Valdes-Korovkin, I., Holub, A., Yudina, A., 2021. Energy-based indicators of soil structure by automatic dry sieving. Soil Tillage Res. 214, 105183.
Georgiou, C.D., Sun, H.J., McKay, C.P., Grintzalis, K., Papapostolou, I., Zisimopoulos, D., Panagiotidis, K., Zhang, G., Koutsopoulou, E., Christidis, G.E., Margiolaki, I., 2015. Evidence for photochemical production of reactive oxygen species in desert soils. Nat. Commun. 6, 7100.
Ghahramani, A., Yoshiharu, I., Mudd, S.M., 2012. Field experiments constraining the probability distribution of particle travel distances during natural rainstorms on different slope gradients. Earth Surf. Processes Landforms 37 (5), 473–485.
Gottselig, N., Bol, R., Nischwitz, V., Vereecken, H., Amelung, W., Klumpp, E., 2014. Distribution of phosphorus-containing fine colloids and nanoparticles in sstream water of a forest catchment. Vadose Zone J. 13 (7) vzj2014.01.0005.
Gottselig, N., Nischwitz, V., Meyn, T., Amelung, W., Bol, R., Halle, C., Vereecken, H., Siemens, J., Klumpp, E., 2017. Phosphorus binding to nanoparticles and colloids in forest stream waters. Vadose Zone J. 16 (3), 1–12.
Greenbaum, N., Mushkin, A., Porat, N., Amit, R., 2020. Runoff generation, rill erosion and time-scales for hyper-arid abandoned alluvial surfaces, the Negev desert, Israel. Geomorphology 358, 107101.
Gu, S., Gruau, G., Malique, F., Dupas, R., Petitjean, P., Gascuel-Odoux, C., 2018. Drying/rewetting cycles stimulate release of colloidal-bound phosphorus in riparian soils. Geoderma 321, 32–41.
Hartmann, A., Weiler, M., Greinwald, K., Blume, T., 2022. Subsurface flow paths in a chronosequence of calcareous soils: impact of soil age and rainfall intensities on preferential flow occurrence. Hydrol. Earth Syst. Sci. 26, 4953–4974.
Hathaway, J.C., 1956. Procedure for clay mineral analyses used in the sedimentary petrology laboratory of the U.S. Geol. Surv. Clay Min. 3 (15), 8–13.
He, Y., Li, D.C., Velde, B., Yang, Y.F., Huang, C.M., Gong, Z.T., Zhang, G.L., 2008. Clay minerals in a soil chronosequence derived from basalt on Hainan Island, China and its implication for pedogenesis. Geoderma 148 (2), 206–212.
Houston, J., 2002. Groundwater recharge through an alluvial fan in the Atacama Desert, northern Chile: mechanisms, magnitudes and causes. Hydrol. Process. 16, 3019–3035.
Houston, J., 2006a. Evaporation in the Atacama Desert: an empirical study of spatio-temporal variations and their causes. J. Hydrol. 330 (3–4), 402–412.
Houston, J., 2006b. The great Atacama flood of 2001 and its implications for andean hydrology. Hydrol. Process. 20 (3), 591–610.

Hu, F., Liu, J., Xu, C., Wang, Z., Liu, G., Li, H., Zhao, S., 2018. Soil internal forces initiate aggregate breakdown and splash erosion. Geoderma 320, 43–51.
Hu, W., Cichota, R., Beare, M., Müller, K., Drewry, J., Eger, A., 2023. Soil structural vulnerability: critical review and conceptual development. Geoderma 430, 116346.
Hu, F., Xu, C., Li, H., Li, S., Yu, Z., Li, Y., He, X., 2015. Particles interaction forces and their effects on soil aggregates breakdown. Soil Tillage Res. 147, 1–9.
Huang, L.M., Zhang, X.H., Shao, M.A., Rossiter, D., Zhang, G.L., 2016. Pedogenesis significantly decreases the stability of water-dispersible soil colloids in a humid tropical region. Geoderma 274, 45–53.
Ilg, K., Dominik, P., Kaupenjohann, M., Siemens, J., 2008. Phosphorus-induced mobilization of colloids: model systems and soils. Eur. J. Soil Sci. 59 (2), 233246.
Iserloh, T., Fister, W., Seeger, M., Willger, H., Ries, J.B., 2012. A small portable rainfall simulator for reproducible experiments on soil erosion. 124, 131–137.
Iserloh, T., Ries, J.B., Arnáez, J., Boix-Fayos, C., Butzen, V., Cerdà, A., Echeverría, M.T., ernández-Gálvez, J., Fister, W., Geißler, C., Gómez, J.A., Gómez-Macpherson, H., Kuhn, N.J., Lázaro, R., León, F.J., Martínez-Mena, M., Martínez-Murillo, J.F., Marzen, M., Mingorance, M.D., Ortigosa, L., Peters, P., Regüés, D., Ruiz-Sinoga, J.D., Scholten, T., Seeger, M., Solé-Benet, A., Wengel, R., Wirtz, S., 2013. European small portable rainfall simulators: a comparison of rainfall characteristics. Catena 110, 100–112.
Fernández-Raga, M., Palencia, C., Keesstra, S., Jordán, A., Fraile, R., Angulo-Martínex, M., Cerdà, A., 2017. Splash erosion: a review with unanswered questions. Earth- Sci. Rev. 171, 463–477.
Jiang, X., Amelung, W., Bol, R., Klumpp, E., 2023. Phosphorus content in water extractable soil colloid over a 2000 years chronosequence of paddy-rice management in the Yangtze River Delta, China. Geoderma 430, 116296.
Jiang, X., Bol, R., Nischwitz, V., Sibers, N., Willbold, S., Vereecken, H., Amelung, W., Klumpp, E., 2015. Phosphorus containing water dispersible nanoparticles in arable soil. J. Environ. Qual. 44, 1772–1781.
Jiang, X., Bol, R., Cade-Menun, B., Nischwitz, V., Bauke, S.L., Vereecken, H., Amelung, W., Klumpp, E., 2017. Colloid-bound and dissolved phosphorus species in topsoil water extracts along a grassland transect from Cambisol to Stagnosol. Biogeosciences 14 (5), 1153–1164.
Jones, E.J., Filippi, P., Wittig, R., Fajardo, M., Pino, V., McBratney, A.B., 2021. Mapping soil slaking index and assessing the impact of management in a mixed agricultural landscape. Soil 7, 33–46.
Jordan, T.E., Lohman, R.B., Tapia, L., Pfeiffer, M., Scott, C.P., Amundson, R., Godfrey, L., Riquelme, R., 2020. Surface materials and landforms as controls on InSAR permanent and transient responses to precipitation events in a hyperarid desert, Chile. Rem. Sens. Environ. 237, 111544.
Kahle, M., Kleber, M., Jahn, R., 2004. Retention of dissolved organic matter by phyllosilicate and soil clay fractions in relation to mineral properties. Org Geochem. 35 (3), 269–276.
Kjaergaard, C., Jonge, L.W., Moldrup, P., Schjønning, P., 2004. Water-dispersible colloids: effects of measurement method, clay content, initial soil matric potential, and wetting rate. Vadose Zone J. 3, 403–412.
Knief, C., Bol, R., Amelung, W., Kusch, S., Frindte, K., Eckmeier, E., Jaeschke, A., Dunai, T., Fuentes, B., Mörchen, R., Schütte, T., Lücke, A., Klumpp, E., Kaise, K., Rethermeyer, J., 2020. Tracing elevational changes in microbial life and organic carbon sources in soils of the Atacama Desert. Global Planet. Change 184, 103078.
Krause, L., Klumpp, E., Nofz, I., Missong, A., Amelung, W., Siebers, N., 2020. Colloidal iron and organic carbon control soil aggregate formation and stability in arable Luvisols. Geoderma 374, 114421.
Lebissonnais, Y., 2016. Aggregate stability and assessment of soil crustability and erodibility: I. Theory and methodology. Eur. J. Soil Sci. 67, 11–21.
Li, F., Zhang, Q., Klumpp, E., Bol, R., Nischwitz, V., Ge, Z., Liang, X., 2021a. Organic carbon linkage with soil colloidal phosphorus at regional and field scales: insights from size fractionation of fine particles. Environ. Sci. Technol. 55, 5815–5825.
Li, G., Fu, Y., Li, B., Zheng, T., Wu, F., Peng, G., Xiao, T., 2018. Micro-characteristics of soil aggregate breakdown under raindrop action. Catena 162, 354–359.
Li, H., Liu, G., Gu, J., Chen, H., Shi, H., Elbasit, M.A.M.A., Hu, F., 2021b. Response of soil aggregate disintegration to the different content of organic carbon and its fractions during splash erosion. Hydrol. Process. 35, e14060.
Liu, J., Xu, C., Hu, F., Wang, Z., Ma, R., Zhao, S., 2021. Effect of soil internal forces on fragment size distributions after aggregate breakdown and their relations to splash erosion. Eur. J. Soil Sci. 72, 2088–2101.
Liu, L., Li, Z., Xiao, H., Wang, B., Nie, X., Liu, C., Ni, L., Wang, D., 2019. The transport of aggregates associated with soil organic carbon under the rain-induced overland flow on the Chinese Loess Plateau. Earth Surf. Proc. Land. 44 (10), 1895–1909.
Li, J., Wang, F., Michalski, G., Wilkins, B., 2019. Atmospheric deposition across the Atacama Desert, Chile: compositions, source distributions, and interannual comparisons. Chem. Geol. 525, 435–446.
Lv, L., Li, Y., Zhou, C., 2023. Mechanistic analysis of splash erosion on loess by single raindrop impact: interaction of soil compaction, water content, and raindrop energy. Biosyst. Eng. 236, 238–247.
Majdalani, S., Michel, E., Di-Pietro, L., Angulo-Jaramillo, R., 2008. Effects of wetting and drying cycles on in situ soil particle mobilization. Eur. J. Soil Sci. 59 (2), 147–155.
Ma, R.T., Guo, W., Hu, F., Xu, C., Liu, G., Zhao, S., Zheng, F., 2022. Effects of soil internal forces on splash detachment and transport of aggregated fragments in Mollisols of Northeast China. Eur. J. Soil Sci. 73, 3273.
Martínez-Mena, M., Castillo, V., Albaladejo, J., 2002. Relations between interrill erosion processes and sediment particle size distribution in a semiarid Mediterranean area of SE of Spain. Geomorphology 45, 261–275.
May, S.M., Meine, L., Hoffmeister, D., Brill, D., Medialdea, A., Wennrich, V., Gröbner, M., Schulte, P., Steininger, F., Deprez, M., v Kock, T., Bubnezer, 2020. Origin and timing of past hillslope activity in the hyper-arid core of the Atacama Desert – the formation of fime sediment lobes along the Chuculay Fault System, Northern Chile. Glob. Planet. Change 184, 103057.
Meadows, D.G., Young, M.H., McDonald, E.V., 2008. Influence of relative surface age on hydraulic properties and infiltration on soils associated with desert pavements. Catena 72, 169–178.
Meshesha, D.T., Tsunekawa, A., Tsubo, M., Haregeweyn, N., Tegegne, 2016. Evaluation of kinetic energy and erosivity potential of simulated rainfall using Laser Precipitation Monitor. Catena 137, 237–243.
Menezes-Blackburn, D., Bol, R., Klumpp, E., Missong, A., Nischwitz, V., Haygarth, P.M., 2021. Citric acid effect on the abundance, size and composition of water-dispersible colloids and its relationship to soil phosphorus desorption: a case study. J. Soil Sci. Plant Nutr. 21, 24362–24446.
Missong, A., Bol, R., Nischwitz, V., Krüger, J., Lang, F., Siemens, J., Klumpp, E., 2018a. Phosphorus in water dispersible-colloids of forest soil profiles. Plant Soil 427, 71–86.
Missong, A., Holzmann, S., Bol, R., Nischwitz, V., Puhlmann, H.V., Wilpert, K., Siemens, J., Klumpp, E., 2018b. Leaching of natural colloids from forest topsoils and their relevance for phosphorus mobility. Sci. Total Environ. 634, 305–315.
Mohanty, S.K., Saiers, J.E., Ryan, J.N., 2015. Colloid mobilization in a fractured soil during dry-wet cycles: role of drying duration and flow path permeability. Environ. Sci. Technol. 49 (15), 9100–9106.
Mohanty, S.K., Saiers, J.E., Ryan, J.N., 2016. Colloid mobilization in a fractured soil: effect of pore-water exchange between preferential flow paths and soil matrix. Environ. Sci. Technol. 50 (5), 2310–2317.
Moradi, G., Bol, R., Trbojevic, L., Missong, A., Mörchen, R., Fuentes, B., May, S.M., Lehndorff, E., Klumpp, E., 2020. Contrasting depth distribution of colloid-associated phosphorus in the active and abandoned sections of an alluvial fan in a hyper-arid region of the Atacama Desert. Global Planet. Change 185, 103090.
Owen, J.J., Dietrich, W.E., Nishiizumi, K., Chong, G., Amundson, R., 2013. Zebra stripes in the Atacama Desert: fossil evidence of overland flow. Geomorphology 182, 157–172.
Pan, Y., Chen, C., Shang, J., 2023. Effect of reduced inherent organic matter on stability and transport behaviors of black soil colloids. Chemosphere 336, 139149.
Pfeiffer, M., Morgan, A., Heimsath, A., Jordan, T., Howard, A., Amundson, R., 2021. Century scale rainfall in the absolute Atacama Desert: landscape response and implications for past and future rainfall. Quat. Sci. Rev. 254, 106797.
Quade, J., Rech, J.A., Latorre, C., Betancourt, J.L., Gleeson, E., Kalin, M.T., 2007. Soils at the hyperarid margin: the isotopic composition of soil carbonate from the Atacama Desert, Northern Chile. Geochim. Cosmochim. Acta 71, 3772–3795.
Regelink, I.C., Voegelin, A., Weng, L., Koopmans, G.F., Comans, R.N.J., 2014. Characterization of colloidal Fe from soils using field-flow fractionation and Fe X-edge X-ray adsorption spectroscopy. Environ. Sci. Technol. 48, 43074–43316.
Reichert, J.M., Norton, L.D., Favaretto, N., Huang, C., Blume, E., 2009. Settling velocity, aggregate stability, and erodibility of soils varying in clay mineralogy. Soil Sci. Soc. Am. J. 73 (4), 1369–1377.
Said-Pullicino, D., Giannetta, B., Demeglio, B., Missong, A., Gottselig, N., Romani, M., Bol, R., Klumpp, E., Celi, L., 2021. Redox-driven changes in water-dispersible colloids and their role in carbon cycling in hydromorphic soils. Geoderma 385, 114894.
Schumacher, M., Christl, I., Scheinost, A.C., Jacobsen, C., Kretzschmar, R., 2005. Chemical heterogeneity of organic soil colloids investigated by scanning transmission X-ray microscopy and C-1s NEXAFS microspectroscopy. Environ. Sci. Technol. 39, 9094–9100.
Schweizer, S.A., Bucka, F.B., Graf-Rosenfellner, M., Kögel-Knabner, I., 2019. Soil microaggregate size composition and organic matter distribution as affected by clay content. 355, 113901.
Séquaris, J.M., Lewandowski, H., 2003. Physicochemical characterization of potential colloids from agricultural topsoils. Colloids Surf. A Physicochem. Eng. Asp 217 (1–3), 93–99.
Siemens, J., Ilg, K., Lang, F., Kaupenjohann, M., 2004. Adsorption controls mobilization of colloids and leaching of dissolved phosphorus. Eur. J. Soil Sci. 55, 253–263.
Shen, J., Smith, A.C., Claire, M.W., Zerkle, A.L., 2020. Unravelling biogeochemical phosphorus dynamics in hyperarid Mars-analogue soils using stable oxygen isotopes in phosphate. Geobiology 18, 760–779.
Shi, P., Thorlacius, S., Keller, T., Schulin, R., 2017. Soil aggregate breakdown in a field experiment with different rainfall intensities and initial soil water contents. Eur. J. Soil Sci. 68 (6), 853–863.
Shi, Z.H., Yue, B.J., Wang, L., Fang, N.F., Wang, D., Wu, F.Z., 2012. Effects of mulch cover rate on interrill erosion processes and the size selectivity of eroded sediment on steep slopes. Soil Sci. Soc. Am. J. 77, 257–267.
Sun, X., May, S.M., Amelung, W., Tang, N., Brill, D., Arenas, F., Contreras, D., Fuentes, B., Bol, R., Klumpp, E., 2023. Water-dispersible colloids distribution along an alluvial fan transect in hyper-arid Atacama Desert. Geoderma 438, 116650.
Sun, X., Amelung, W., Klumpp, E., Walk, J., Mörchen, R., Böhm, C., Moradi, G., May, S. M., Tamburini, F., Wang, Y., Bol, R., 2024. Fog controls biological cycling of soil P in the Coastal Cordillera of the Atacama Desert. Glob. Chang. Biol. 30, e17068.
Tanner, S., Kartra, I., Argaman, E., Ben-Hur, M., 2021. Mechanisms and process affecting aggregate stability and saturate hydraulic conductivity of top and sublayers in semi-arid soils. Geoderma 404, 15304.
Tian, Y., Shi, C., Malo, C.U., Kengdo, S.K., Heinzle, J., Inselsbacher, E., Ottner, F., Borken, W., Michel, K., Schindlbacher, A., Wanek, W., 2023. Long-term soil warming decreases microbial phosphorus utilization by increasing abiotic phosphorus sorption and phosphorus losses. Nat. Commun. 14, 864.
Totsche, K.U., Amelung, W., Gerzabek, M.H., Guggenberger, G., Klumpp, E., Knief, C., Lehndorff, E., Mikutta, R., Peth, S., Prechtel, A., Ray, N., Kögel-Knabner, I., 2018. Microaggregates in soils. J. Plant Nutr. Soil Sci. 181, 104–136.

Torkzaban, S., Bradford, S.A., Vanderzalm, J.L., Patterson, B.M., Harris, B., Prommer, H., 2015. Colloid release and clogging in porous media: effects of solution ionic strength and flow velocity. J. Contam. Hydrol. 181, 161–171.
Vaezi, A.R., Ahmadi, M., Cerdà, A., 2017. Contribution of raindrop impact to the change of soil physical properties and water erosion under semi-arid rainfalls. Sci. Total Environ. 583, 382–392.
van den Bogaert, R., Cornu, S., Michel, E., 2016. To which extent do rain interruption periods affect colloid retention in macroporous soils? Geoderma 275, 40–47.
VandeVoort, A.R., Livi, K.J., Arai, Y., 2013. Reaction condictions control soil colloid faciliated phosphorus release in agricultural Ultisols. Geoderma 206, 101–111.
Vereecken, H., Amelung, W., Bauke, S.L., Bogena, H., Brüggemann, N., Montzka, C., Vanderborght, J., Bechtold, M., Blöschl, C., Carminati, A., Javaux, M., Konings, A., Kusche, J., Neuwiler, I., Or, D., Steele-Dunne, S., Verhoef, A., Young, M., Zhang, Y., 2022. Soil hydrology in the Earth system. Nat. Rev. Earth Environ. 3, 573–587.
Voigt, C., Klipsch, S., Herwartz, D., Chong, G., Staubwasser, M., 2020. The spatial distribution of soluble salts in the surface soil of the Atacama Desert and their relationship to hyperaridity. Global Planet. Change 184, 103077.
Walk, J., Schulte, P., Bartz, M., Binnie, A., Kehl, M., Mörchen, R., Sun, X., Stauch, G., Tittmann, C., Bol, R., Brückner, H., Lehmkuhl, F., 2023. Pedogenesis at the coastal arid-hyperarid transition deduced from a Late Quaternary chronosequence at Paposo, Atacama Desert. Catena 228, 107171.
Wang, C., Wang, R., Huo, Z., Xie, E., Dahlke, H.E., 2020a. Colloid transport through soil and other porous media under transient flow conditions-a review. WIREs Water 7, e1439.
Wang, F., Michalski, G., Seo, J., Ge, W., 2014a. Geochemical, isotopic, and mineralogical constrains on atmospheric deposition in the hyper-arid Atacama Desert, Chile. Geochim. Cosmochim. Acta 135, 29–48.
Wang, L., Missong, A., Amelung, W., Willbold, S., Prietzel, J., Klumpp, E., 2020b. Dissolved and colloidal phosphorus affect P cycling in calcareous forest soils. Geoderma 375, 114507.
Wang, Y., Moradi, G., Klumpp, E., Sperber, C., Tamburini, F., Ritter, B., Fuentes, B., Amelung, W., Bol, R., 2021a. Phosphate oxygen isotope fingerprints of past biological activity in the Atacama Desert. Geochim. Cosmochim. Acta 311, 1–11.
Wang, L., Shi, Z., Wang, J., Fang, N., Wu, G., Zhang, H., 2014b. Rainfall kinetic energy controlling erosion processes and sediment sorting on steep hillslopes: a case study of clay loam soil from the Loess Plateau, China. J. Hydrol. 512, 168–176.
Wang, Z., Chen, L., Liu, C., Jin, Y., Li, F., Khan, S., Liang, X., 2021. Reduced colloidal phosphorus loss potential and enhanced phosphorus availability by manure-derived biochar addition to paddy soils. Geoderma 402 (15), 115348.
Wang, Z., Eltohamy, K.M., Liu, B., Jin, J., Liang, X., 2024. Effects of drying-rewetting cycles on colloidal phosphorus composition in paddy and vegetable soils. Sci. Total Environ. 907, 168016.
Weber, F.A., Voegelin, A., Kaegi, R., Kretzschmar, R., 2009. Contaminant mobilization by metallic copper and metal sulphide colloids in flooded soil. Nat. Geosci. 2, 267–271.
Xiao, H., Liu, G., Abd-Elbasit, M.A.M., Zhang, X.C., Liu, P.L., Zheng, F.L., Zhang, J.Q., Hu, F.N., 2017. Effects of slaking and mechanical breakdown on disaggregation and splash erosion. Eur. J. Soil Sci. 68 (6), 797–805.
Xie, H., Wu, L., Xie, W., Lin, Q., Liu, M., Lin, Y., 2021. Improving ECMWF short-term intensive rainfall forecasts using generative adversarial nets and deep belief networks. Atmos. Res. 249, 105281.
Yu, M., Gan, Z., Zhang, W., Yang, C., Zhang, Y., Tang, A., Dong, X., Yang, H., 2024. Differential adsorption of dissolved organic matter and phosphorus on clay mineral in water-sediment system. Environ. Sci. Technol. 58 (4), 2078–2088.
Zambon, N., Johannsen, L.L., Strauss, P., Dostal, T., Zumr, D., Cochrane, T.A., Klik, A., 2021. Splash erosion affected by initial soil moisture and surface conditions under simulated rainfall. Catena 196, 104827.
Zhang, Q., Bol, R., Amelung, W., Missong, A., Siemens, J., Mülder, I., Willbold, S., Muller, C., Westphal Muniz, A., Klumpp, E., 2021. Water dispersible colloids and related nutrient availability in amazonian Terra Preta soils. Geoderma 397, 115103.
Zhang, Q., Boutton, T.W., Hsiao, C.J., Mushinski, R.M., Wang, L., Bol, R., Klumpp, E., 2023. Soil colloidal particles in a subtropical savanna: biogeochemical significance and influence of anthropogenic disturbances. Geoderma 430, 116282.
Zhang, W., Tang, X., Xian, Q., Weisbrod, N., Yang, J.E., Wang, H., 2016. A field study of colloid transport in surface and subsurface flows. J. Hydrol. 524, 101–114.
Zomer, R.J., Xu, J., Trabucco, A., 2022. Version 3 of the global aridity index and potential evapotranspiration database. Sci. Data 9, 409.